UNIVERSITÀ DEGLI STUDI DI MILANO

DOTTORATO DI RICERCA IN MEDICINA TRASLAZIONALE XXXVI CICLO

Dipartimento di Scienze Biomediche per la Salute

AGE-RELATED GUT DYSBIOSIS ACCELERATES THYMIC INVOLUTION AND ALTERS PERIPHERAL T CELL REPERTOIRE IN DUCHENNE MUSCULAR DYSTROPHY

MED/26 - NEUROLOGIA

DOTTORANDA

Luana TRIPODI

Matricola n. R12847

TUTOR

Prof. Yvan TORRENTE

COORDINATORE DEL DOTTORATO

Prof.ssa Chiarella SFORZA

Anno Accademico 2022 - 2023

INDEX

ABSTRACT

Emerging researches highlight a significant interplay between the immune system and skeletal muscle, particularly in the context of inflammatory muscle disorders and dystrophic conditions like Duchenne Muscular Dystrophy (DMD), as well as during the natural process of muscle regeneration. Conventionally, immune system activation was regarded as a consequence of muscle atrophy. However, recent findings have unveiled a malfunction in central tolerance due to thymus alterations and the presence of autoreactive T-lymphocytes in patients with DMD. Moreover, the development and equilibrium of both innate and adaptive immune systems have become increasingly linked to the microbiota, the microorganisms inhabiting the gut. For this purpose, we investigated the role of the commensal microbiota in exacerbating muscle damage via immune system activation. We created a network of expertise to characterize the intestinal environment and its microbial ecology in murine models of muscular dystrophies and we proposed that alterations of commensal communities actively contribute to disease pathogenesis by a combination of adaptive and innate pathways. We also investigated whether healthy and dystrophic aging lead to the proliferation of pathobionts or protective taxa, as well as microorganisms contributing to muscle degeneration and inflammation. Overall, this study provide valuable insights into how the intestinal microbiota shapes the inflammatory response, thereby conferring distinct susceptibility to muscle pathology. Furthermore, we potentially identified novel biomarkers associated with gastrointestinal involvement and disease progression prediction, which could be translated into human studies and aid in stratifying patients based on the most appropriate treatments.

INTRODUCTION

Muscular dystrophies (MDs) are a group of neuromuscular diseases characterized by progressive muscle damage and wasting of skeletal muscle tissue, which involves patient mobility, respiratory and cardiac functionality leading to premature death[1]. The classification is based both on the resulting expressed protein and on their localization and function[2] and several forms of MDs can be distinguished: Duchenne Muscular Dystrophy (DMD), Becker Muscular Dystrophy (BMD), Emily-Dreifuss Muscular Dystrophy, Facioscapulohumeral Muscular Dystrophy (FSHD), Oculopharyngeal and Limb-girdle Muscular Dystrophies (LMGD) (Fig. 1).

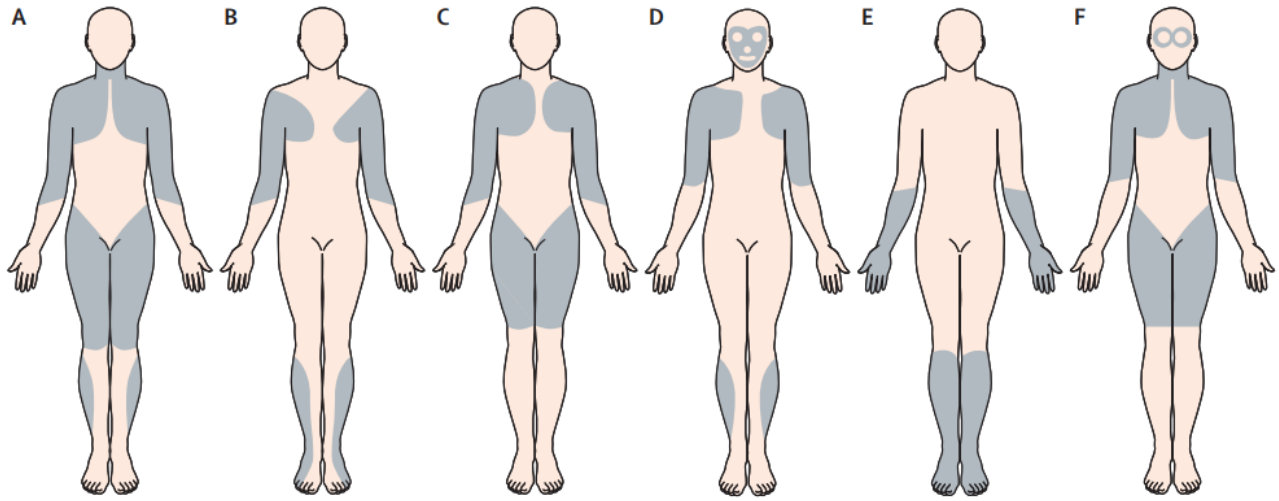

Figure 1. (A) Duchenne and Becker muscular dystrophy. (B) Emery-Dreifuss muscular dystrophy. (C) Limb girdle muscular dystrophy. (D) Facioscapulohumeral muscular dystrophy[2]. (E) Distal, (F) oculopharyngeal.

DUCHENNE MUSCULAR DYSTROPHY

DMD is an X-linked disease caused by mutations in the DMD gene, leading to a truncated and unstable dystrophin protein and myofiber membrane fragility and necrosis[3]. Normal skeletal muscle consists of muscle fibers that are evenly spaced and uniform in size and, being a syncytium, is multinucleated with nuclei located at the periphery of the fiber. All postnatal DMD muscle biopsies reveal necrotic and degenerating muscle fibers: these degenerating/necrotic fibers are often seen in clusters and are subject to phagocytosis, showing the presence of inflammatory cells at the perimysial and endomysial sites (Fig. 2). Another sign of muscle fiber necrosis, at the early stages, is the activation of regenerative pathways trying to repair damaged fibers. Early regenerating fibers are recognized by their small diameter, basophilic RNA-rich cytoplasm, and large, centrally placed myonuclei. The lack of regenerative capacity leads to gradual replacement of the fibers with adipose and fibrous connective tissue, giving rise to the clinical appearance of

pseudohypertrophy followed by atrophy condition. Finally, progressive fibrosis and continued muscle fibers loss result in muscular wasting and weakness[4]. In addition to muscular symptoms, cognitive impairment also develops, resulting from defects in the synaptic function of the Central Nervous System organization and loss of neurons. Moreover, after 10 years of age, clinically apparent cardiomyopathy is evident, affects one-third of patients by the age of 14 and all patients over 18 years of age. Cardiorespiratory failures are the most common causes of death in DMD patients[5,6]: death takes place at around 20-30 years of age.

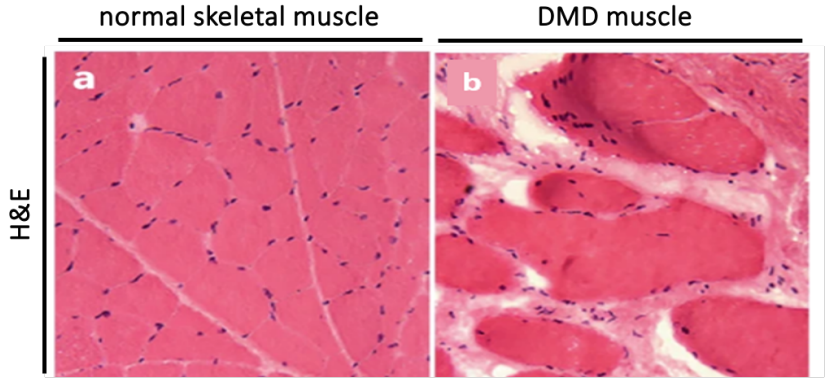

Figure 2. Hematoxylin and Eosin (H&E) staining of normal skeletal muscle (a) and DMD muscle (b)

DYSTROPHIN GENE

The DMD gene, discovered by positional cloning, is the largest known gene with a 2.5 MB and is encoded on the X chromosome (Xp21). It spans a total of 79 exons and encodes a ~14-kb cDNA[7] (Fig. 3). The dystrophin gene has seven promoters known to initiate protein transcription and three of these generate full-length dystrophin transcripts: the M promoter produces the Dp427m isoform, expressed in skeletal and cardiac muscle; the B promoter produces Dp427c, expressed in the brain; the P promoter produces Dp427p, expressed in the Purkinje cell in the brain. The remaining four tissue-specific promoters regulate the N-terminus truncated short isoforms: Dp260, Dp140, Dp116, and Dp71. Dp260 is expressed in high concentrations in the retina. Brain, retina, and kidneys tissues express Dp140. Adult peripheral nerves express Dp116. Dp71 is found in cardiac muscle but absent in skeletal muscle, and it is found in the majority of brain, retina, kidney, liver, and lung[8]. Dp427m is responsible for DMD and BMD and it is expressed mainly in skeletal and cardiac muscle. MDs are caused by mutations in one or several of the 79 exons of dystrophin, in particular the mutations in DMD result in a prematurely truncated, unstable dystrophin protein. Most DMD patients have a deletion as a mutation, which accounts for 65–70% of all mutations. Most commonly, deletions occur in two 'hotspot' mutational regions: the first

region spanning exons 45–53 and the second one is localized between exon 2 and exon 19. Duplications are found in 7% of all patients and point mutations or small deletions/insertions are found in the remainder[9] .

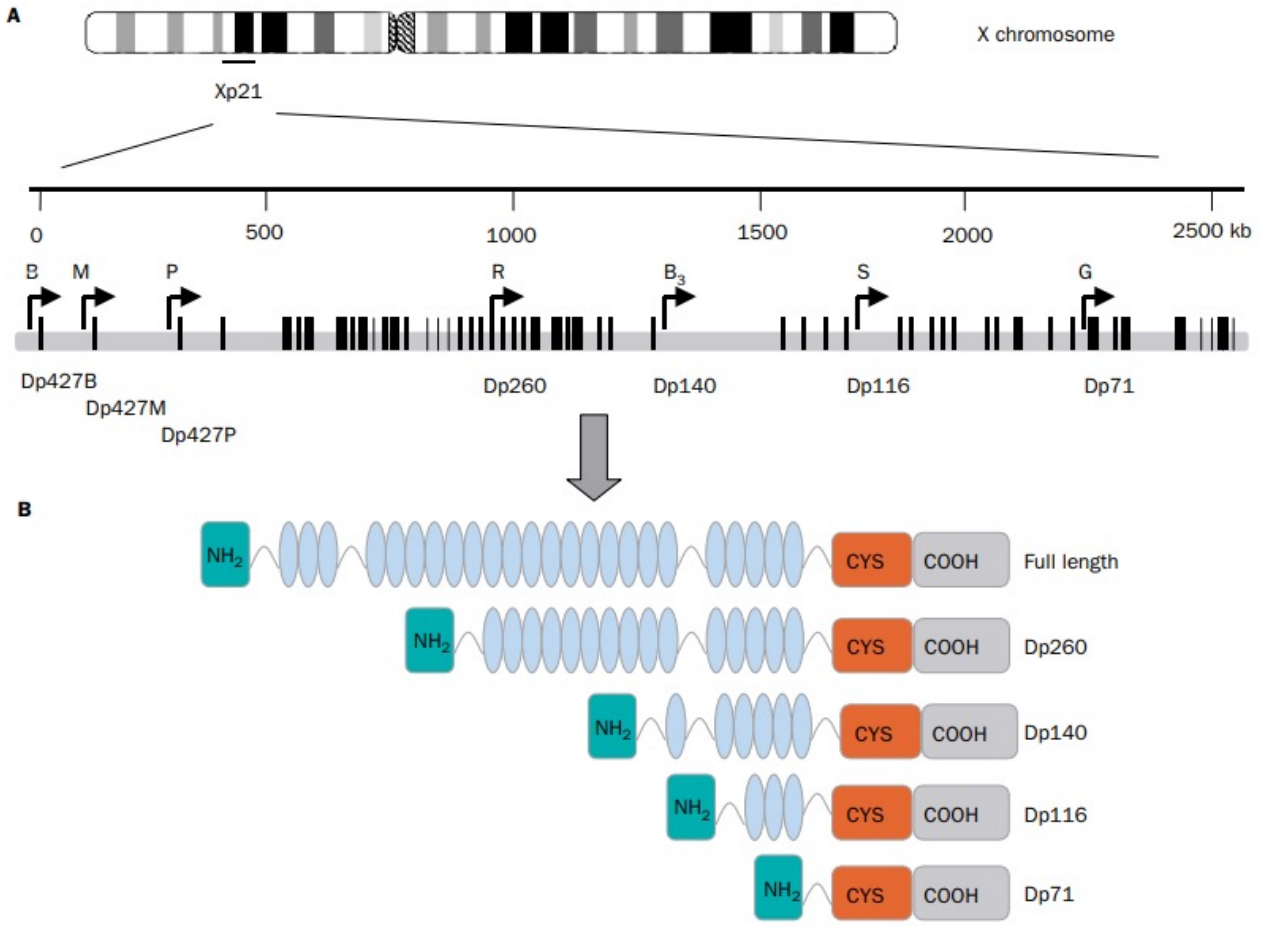

Figure 3. Genomic organization of the dystrophin gene, located in Xp21. The black vertical lines represent the 79 exons of the dystrophin gene and the arrows represent the different promoters (a). Representation of the different dystrophin isoforms (b)[10].

DYSTROPHIN PROTEIN

Dystrophin is a large rod-shaped cytoskeletal protein that is a member of the beta-spectrin/alpha-actinin protein family. This family is characterized by an NH2-terminal actin-binding domain followed by a variable number of repeating units known as spectrin-like repeats[11] . Dystrophin contains about 3685 amino acids with a molecular weight of 427 KDa, it localizes to the cytoplasmic face of the sarcolemma and is enriched at the costameres in muscle fibers[12]. It is composed of four structural domains based on sequence homologies and protein-binding capabilities. The NH2-terminal domain consisting of 220 aminoacidic residues binds F-actin, linking dystrophin to the

subsarcolemmal actin network. The rod domain consists of 24 repeating units with α-helical secondary spectrin-like structures; the α-helical coiled coil repeats are separated by four proline hinge regions. The 24 repeating units account for most of the dystrophin protein and are thought to give the molecule a flexible rodlike structure like beta-spectrin, they are also required for the organization of microtubule in skeletal muscle cells. This proline hinge region is followed by a domain made up of two conserved Triptofan residues (WW) and a Proline one, which are responsible for mediating interactions between dystrophin and β-dystroglycan and function as an identification unit for regulatory molecules[13]. The rod domain confers a huge flexibility to dystrophin, a property required to maintain an efficient structural bridge between the extracellular matrix and the sarcomeres. Another important region is the cysteine-rich domain which contains two EF-hand helix-loop-helix motifs able to bind the intracellular Ca2+ and the ZZ domain which contains cysteine residues which bind to the calmodulin in the presence of Ca2+ allowing interaction between the calmodulin and other dystrophin proteins. The COOH terminal domain consists of helical coiled coil regions and connects the proteins associated with dystrophin such as dystrobrevin and syntrophin to the sarcolemma: it binds to F-actin through the amino-terminal domain, while it binds to β-dystroglycan through the carboxyl-terminal domain and acts as an anchor point for the dystrophin-associated glycoprotein complex (DAGC) at the sarcolemma[14] (Fig. 4). In this way it functions as a linker between the intracellular space and the extracellular matrix (ECM) conferring mechanical resistance during muscle contraction. Beyond the linker activity, dystrophin within the cell shows numerous diverse functions, one of the most important is that DAGC is involved in signaling, in fact it is involved in the localization of neuronal nitric oxide synthase (nNOS) at the level of the sarcolemma. In skeletal muscle, the nNOS plays an important role in the regulation of many muscle functions, including blood flow, contraction, and muscle metabolism. NOS localized in the sarcolemma enhances blood flow and oxygen delivery, thereby more efficiently matching the blood supply to the metabolic demands of active muscle[15]. Among other functions, dystrophin is also involved in the essential signaling platform that orchestrates membrane lipids and proteins (cholesterol, cavins, ion channels, caveolins and G protein coupled receptors). For this reason, mutations with dystrophin loss cause muscle wasting and mechanical damage sensitivity and damage to the membrane[16] with an increased intracellular calcium influx, dysregulated cellular signaling, mitochondrial malfunctioning, and an inadequate antioxidant response. All these conditions have fiber necrosis and the activation of an inflammatory response[17]

as result.

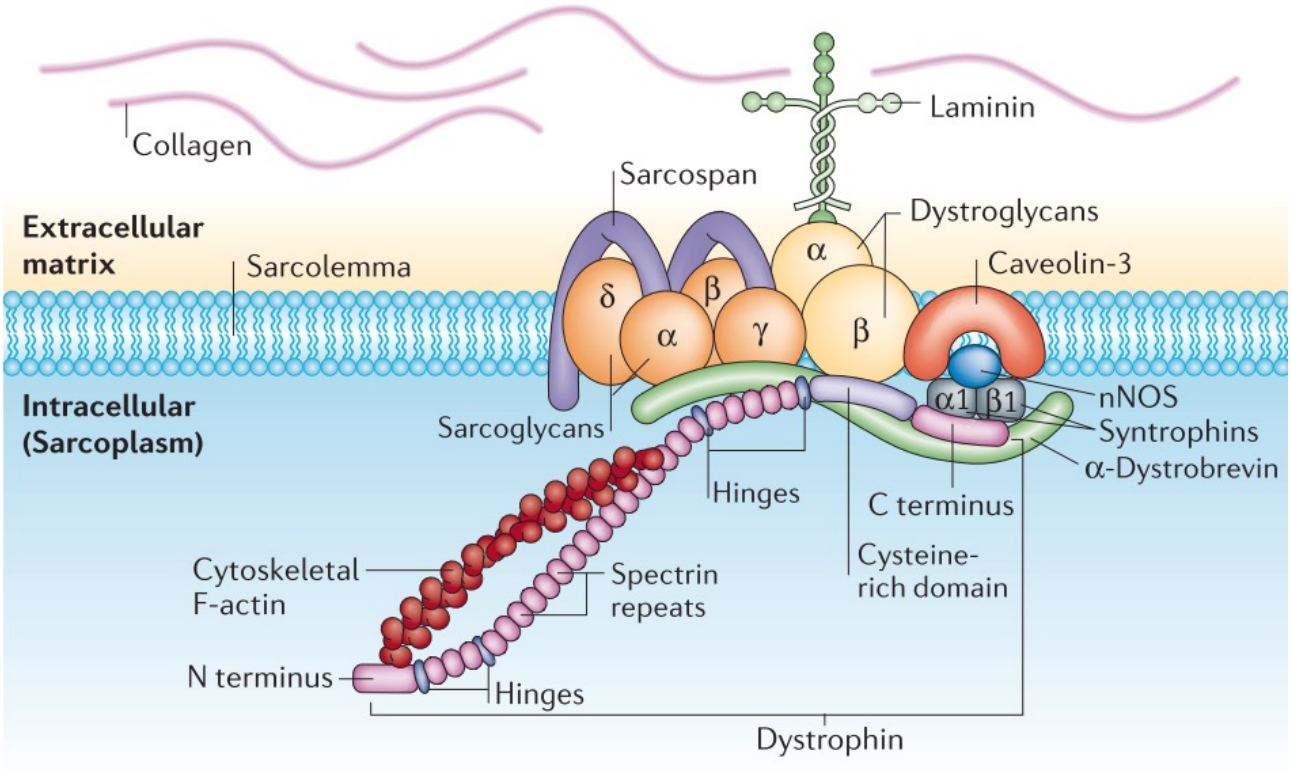

Figure 4. The dystrophin-associated protein complex. This image shows how Dystrophin acts as an important link between the internal cytoskeleton and the extracellular matrix (From: The Extracellular Matrix An Overview; Jeffrey H. Miner, Chapter: Basement Membranes*).*

ANIMAL MODEL OF DUCHENNE MUSCULAR DYSTROPHY

Dystrophin-deficient mdx mouse which was described for the first time in 1984[18] and it is the result of a spontaneous mutation which occurred in an inbred colony of C57BL/10 mice[19]. Examination of mdx skeletal muscle shows progression in necrosis at around 3 weeks of post-natal life, followed by an extensive period of degeneration and regeneration (starting at 2 weeks, peaking at 12 months, continuing for the life of mdx). Necrotic process gradually decreases, remaining at a relatively low level in adult mice (3-4 months) due to pathology stabilization[20]. Chronic inflammation, as evidenced by the infiltration of inflammatory cells, is found in mdx peripheral skeletal muscles, such as in DMD. Another sign in DMD patients and in mdx mice is myocardial fibrosis. This process begins at 2 months of age in mdx mice with cardiac dysfunction and morphological changes detected from 8 months of age. Connective tissue accumulates in mdx hearts, suggesting that fibrosis can lead to some features of the cardiomyopathy[6]. The similarity in pathological phenotype of DMD leads us to use mdx murine model for our studies. Four chemical variation (cv) mdx strains were released in 1989. These mice, known as mdx2cv, mdx3cv,

mdx4cv, and mdx5cv, were produced on the C57BL/6 background using the mutagen N-ethyl-N-nitrosourea (ENU) and they differ in the point mutations. For example, a point mutation in intron 65 causes incorrect splicing and impaired production of a disrupted dystrophin in mdx3cv mice, while a nonsense point mutation in exon 53 causes premature translation termination in mdx4cv mice[21]. Each line has distinct characteristics, even though the clinical presentation is remarkably similar to mdx mice. mdx5cv mice have a more severe skeletal muscle phenotype; mdx4cv and mdx5cv mice rarely have revertant fibers. Apart from the strains already mentioned, multiple other lines lacking in dystrophin (Dup2, MD-null, Dp71-null, mdx52, and mdx βgeo) have been generated by diverse genetic engineering methodologies[22].

INNATE IMMUNE SYSTEM IN MUSCULAR DYSTROPHY

Inflammation and innate immune response activation are firstly a consequence of the physiological function of skeletal muscle, but their chronic activation is determined by a continuous cycle of muscle fiber degeneration/regeneration. Under physiological conditions, skeletal muscle contains resident immune cells, mainly macrophages, which play multiple roles such as phagocytosis of cellular debris and microbes, secretion of cytokines and growth factors, antigen-presentation. Following pathophysiological stimuli, the skeletal muscle is invaded by several immune cells that secrete soluble molecules, affecting the viability and transcriptional activities of regenerative muscle cells. Muscle innate immune response to injury is mediated by Th1 cytokines (cytokines expressed by T helper cells subset). These cytokines, such as the tumor necrosis factor-α (TNF-α), trigger the activation of M1 proinflammatory macrophages, which in turn promote the production of prostaglandins, cytokines, and chemokines. Following the early invasion of macrophages/neutrophils, TNF- α is highly expressed, activating macrophages in the M1 phenotype and inducing the production of other proinflammatory cytokines. This inflammatory condition is essential for activating the Nuclear Factor Kappa-light-chain-enhancer of activated B cells (NF-kB). NF-kB allows the expression of the transcripts needed for cell cycle progression therefore increasing proliferation and inhibiting differentiation of muscle stem cell, through the destabilization of MyoD mRNA and the degradation of MyoD protein. We know that cells must stop proliferation to differentiate and that MyoD is important for the differentiation, so NF-kB negatively affects the capacity of muscle at terminal differentiation[23]. There must be sufficient proliferation of satellite cells to repair an injured site before myogenic differentiation begins. Recent discoveries reveal that TNF-α secretion in the injury site is necessary to attract the satellite cells (SCs) in situ

and, thus, to promote muscle regeneration. When M1 macrophages reached their peak of concentration in injured/regenerative muscle, Th2 cytokines (such as the interleukins IL-4, IL-10 and IL-13) stimulation promotes a switch toward M2 anti-inflammatory macrophages, which decreases the inflammatory response and promotes tissue repair[23]. Conversely, the continuous activation of regenerative process leads to the rising of inflammation, with the activation of the immune system and the consequent infiltration of inflammatory cell population, promoting muscle damage and the activation of fibrotic process[24] (Fig. 5).

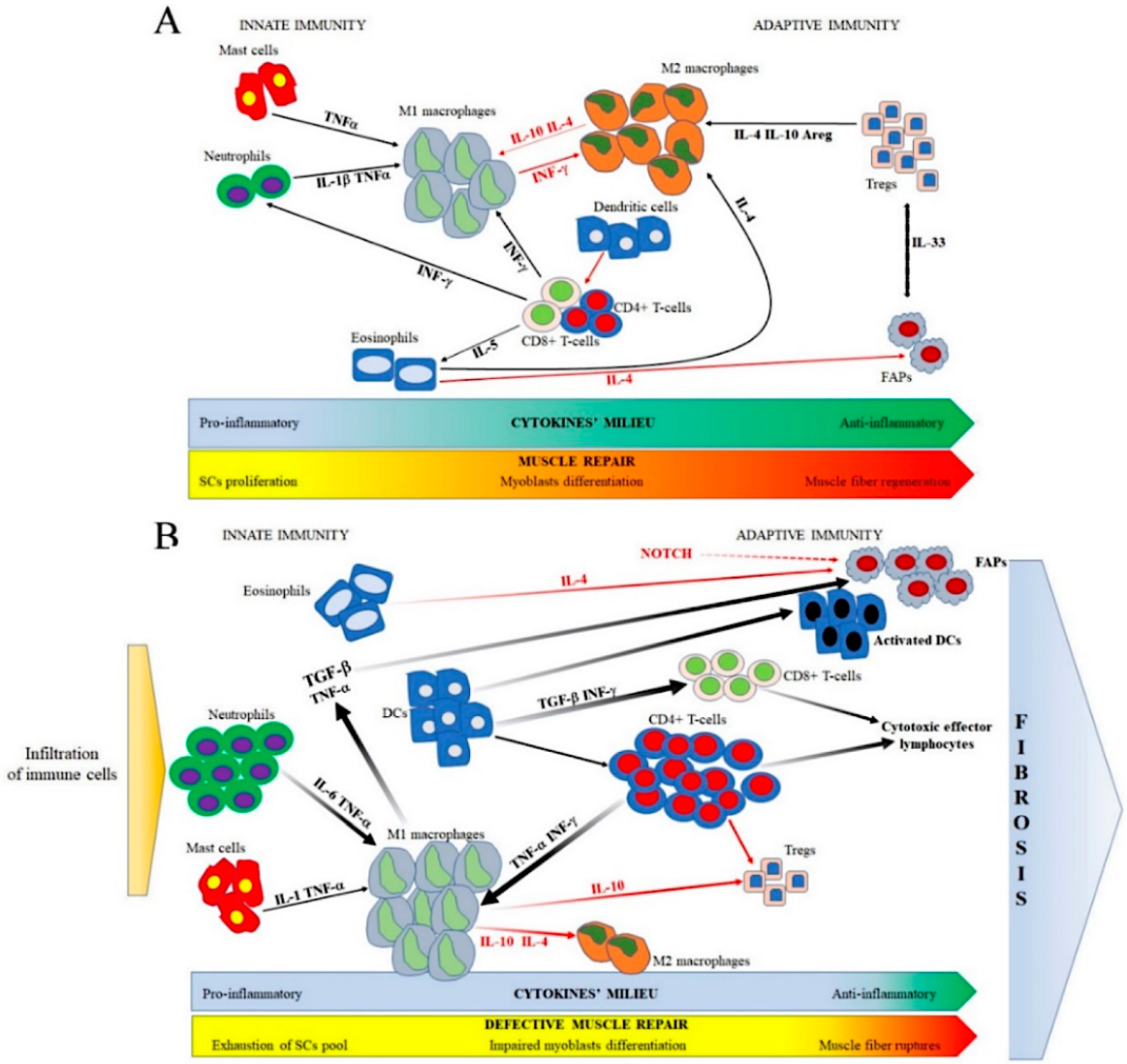

Figure 5. (A) In the initial phase of muscle repair in healthy subjects, a well-balanced innate immune response regulates the expression of pro-inflammatory cytokines like IL-6, TNFα, and IL-1. These cytokines are essential for inducing muscle fiber necrosis and clearing cellular debris by activating M1 macrophages. The secretion of anti-inflammatory mediators such as IL-4, IL-10, and Areg facilitates the transition of macrophages towards an M2 phenotype, stimulates Treg proliferation, and establishes a connection between Tregs and FAPs through IL-33 expression. These coordinated processes result in the resolution of inflammation and muscle regeneration. (B) In a dystrophic context, degenerating

dystrophin-deficient fibers release pro-inflammatory cytokines and chemokines, leading to the recruitment of mast cells and neutrophils to the muscles. These cells, in turn, activate the proliferation of M1 macrophages. Concurrently, professional antigen-presenting cells (APCs) such as dendritic cells (DCs) activate CD4+ and CD8+ lymphocytes, which contribute to the release of TNFα, IL-6, and INF-γ and evolve into cytotoxic T-cells. In this scenario, the inflammatory milieu results in the down-regulation of IL-10, IL-4, and Areg, inhibiting the presence of anti-inflammatory cells like M2 macrophages and Tregs. The overexpression of TGF-β, mediated by M1 macrophages, activates fibro-adipogenic progenitors (FAPs), whose proliferation is driven by eosinophils due to the scarcity of IL-4. All of these cell types collectively disrupt muscle homeostasis, promote muscle necrosis, and contribute to fibrosis. Cytokines with inhibitory effects are highlighted in red, while activating cytokines are highlighted in black, with arrow thickness corresponding to the cytokine abundance in both normal and pathological muscle conditions[6].

FIBROSIS IN MUSCULAR DYSTROPHY

Fibrosis is the result of a reactive or reparative process involving mechanical, humoral, and cellular factors. Fibrosis originates from vulnerable myofibers, muscle cells in necrosis and inflammatory processes which are present in DMD[25] (Fig. 6). Fibrosis is characterized by an excessive deposition of extracellular matrix (ECM) proteins with the proliferation and activation of myofibroblasts, including collagens and fibronectin that can impair tissue function[26 27]. It was demonstrated that Toll-Like Receptor (TLR) activation is an important link between the innate and adaptive immune responses and it was shown to be expressed in the major antigen-presenting cells, dendritic cells (DCs)[28]. TLRs are prototype pattern-recognition receptors (PRRs) that discern pathogen associated molecular patterns (PAMPs) from microorganisms, and DAMPs from damaged tissue. DAMPs include several molecules, the most important are the alarmins. Alarmins are chemotactic, endogenous, constitutively expressed proteins/peptides that are released following cell injury or death to trigger a rapid response by immune cells. These proteins are said to exert dual-function proteins that have distinct roles inside or outside the cells. This group of proteins includes the high-mobility group box 1 protein (HMGB1), IL-1α, IL-33 and the $Ca2^{+}$-binding S100 proteins[29]. TLR signaling pathways activation is mediated through intracytoplasmic TIR domains, which are conserved among all TLRs. Recent studies have demonstrated that TIR domain-containing adaptors, such as MyD88, TIRAP, and TRIF, modulate TLR signaling pathways. In the MyD88-dependent pathway, upon TLR activation, MyD88 interacts with the death domains of members of the IRAK (IL-1 receptor-associated kinase), leading to the activation of TRAF6 factor. These interactions recruit a protein kinase complex involving TAK1 (transforming growth factor-b-activated kinase-1, TGFβ Activated Kinase) and TABs (TAK1 binding proteins) (TAB1, TAB2 and TAB3), which then activate two distinct pathways involving the IKK complex and the mitogen-

activated protein kinase (MAPK) (ERK, JNK, p38) pathway. TLR pathways ends in NF-kB activation, which controls the expression of numerous inflammatory cytokines and pro-fibrotic genes[30]. One of the target genes of NF-kB is the fibronectin gene. Fibronectin (FN) is a glycoprotein of the connective tissue and expressed on the cell surface together with, collagen, glycosaminoglycans and proteoglycans. It is synthesized by many types of differentiated cells and is involved in the attachment of cells to the surrounding extracellular matrix. The cells found in fibrous tissue are mainly fibrocytes and myofibroblasts. Precursor cells differentiate into these cell types through various stimulators. One of them is the transforming growth factor-β (TGF-β). TGF-β increases ECM deposition by stimulating synthesis of matrix proteins, reducing production of matrix-degrading proteases, and modulating expression of ECM receptors on the cell surface. Fibrosis has a double negative consequence for the potential treatment of DMD since it not only alters muscle function, but also reduces the amount of target muscle available for therapy and repair[31].

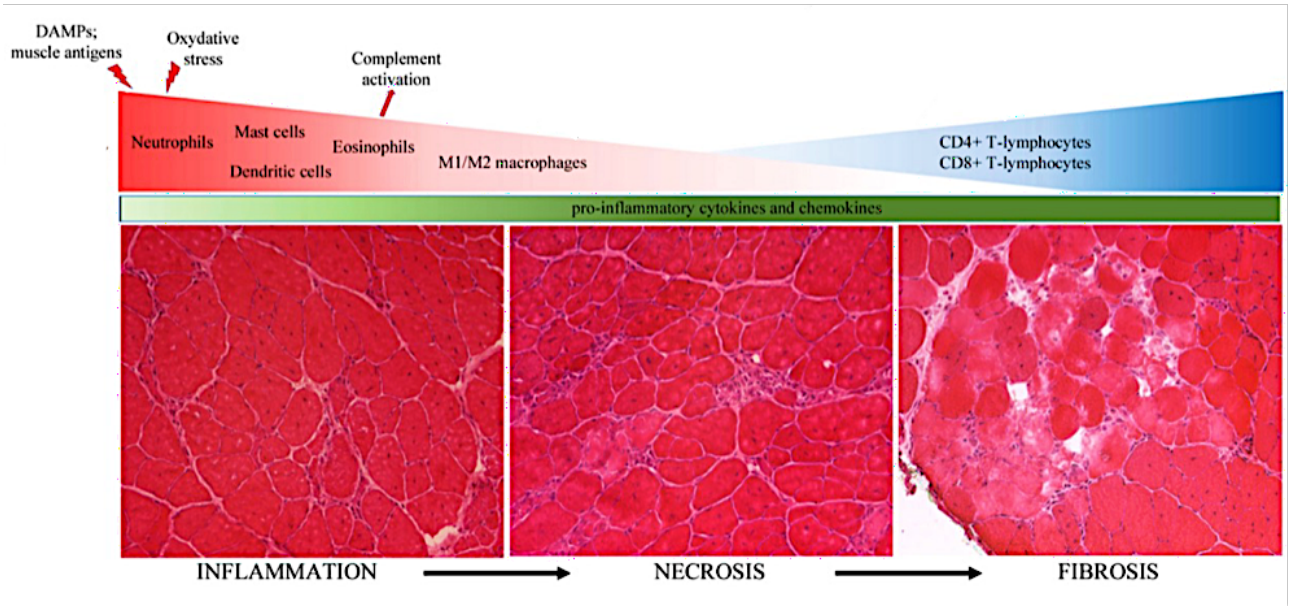

Figure 6. The absence of dystrophin results in the destabilization of cell membranes, leading to uncontrolled leakage of cytoplasmic contents into the surrounding extracellular matrix. These processes initiate the destruction of muscle fibers and trigger a persistent activation of the innate immune system. Damage-associated molecular patterns (DAMPs) are released, while muscle antigens stimulate the recruitment of neutrophils, followed by the rapid involvement of M1 macrophages and eosinophils. These immune cells release pro-inflammatory cytokines and free radicals, contributing to an increase in oxidative stress and the characteristic inflammatory environment seen in DMD muscles. This condition leads to a subsequent wave of infiltration by inflammatory cells, primarily comprised of CD4+ and CD8+ cytotoxic T-lymphocytes. The unresolved inflammation ultimately results in muscle fiber necrosis and, subsequently, the replacement of muscle tissue by adipose cells, which is a major contributor to muscle weakness[32].

THYMUS AND ADAPTIVE IMMUNE SYSTEM IN MUSCULAR DYSTROPHY

In DMD, muscle degeneration is caused by inflammation and cellular infiltration triggered by damage-associated molecular patterns (DAMPs) resulting from damaged muscle fibers, oxidative stress, and impaired calcium handling. However, specific activation of adaptive immunity has also been observed in DMD subjects. Mendell *et al* found the presence of circulating CD4+ T cells reactive against self-dystrophin epitopes in two patients before functional dystrophin transgene vector treatment[33]. Similarly, Flanigan *et al* demonstrated the presence of a spontaneously developed T-cell-mediated immune response against dystrophin in one-third of the 70 patients in the DMD cohort[34]. Based on this, it is possible that in DMD patients not all dystrophin-reactive T cells are correctly deleted in the thymus, leading to a T cells activation by revertant myofibers expressing dystrophin protein[35-37]. Normally, the thymus produces mature T lymphocytes from bone marrow-derived cells, screening them for autoreactivity (Fig. 7). Thymic immune activity is compromised by aging process, which leads to a continuous loss of thymic epithelial cells (TECs), determining a thymic involution[38,39]. This condition causes impaired negative selection of self-reactive T cells and an autoimmune response activation with tissue damage and chronic inflammation. TECs are important fot the maintenance of thymic architecture and functionality and they can be divided into cortical TECs (cTECs) and medullary TECs (mTECs). cTECs are involved in early T cell differentiation process, while mTECs are important to establish the self-tolerance through negative selection and generation of regulatory T cells. Since it is known thymus is important to maintain immunity reaction[40,41], in the first year of my PhD program, we investigated mdx thymic structure and we observed that it is severely altered, correlating to ghrelin (GHR) expression and autophagy activation with a dysfunction of the GHR-GHR axis receptor (GHS-R)[42]. Moreover, we demonstrated that transplantation of mdx thymus in nude mice increased the expression of inflammation-fibrosis and metabolic breakdown markers, suggesting that degeneration of the dystrophic thymus exacerbates muscular dystrophy by impairing central immune tolerance. This represent the first evidence that impaired immune system activation is a primitive feature of MD independently from genetic muscle defects. Indeed, the age-related changes that normally affect thymus functions drastically deteriorate both negative selection and Treg induction: all these events determine self-tolerance breakdown and alterations in T cell development and differentiation. In particular, aging can lead to accumulation of specialized mTECs that express myogenic markers like the myoid cells, preventing central tolerance thus causing the development of autoimmunity; the amount of thymocyte is reduced due to the rising of

inflammation and oxidative stress; the accumulation of adipose tissue in thymus parenchyma as well as altered glycosylation all dramatically impaired immune homeostasis.

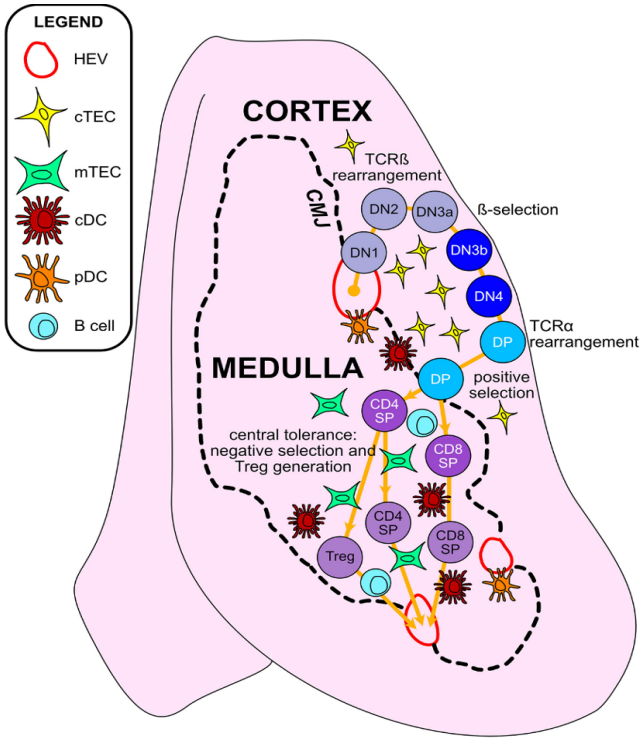

Figure 7. Thymic epithelial cells and hematopoietic antigen-presenting cells play a crucial role in guiding the maturation of αβT cells and inducing central tolerance within the thymus[43].

GUT-MICROBIOTA IN MUSCULAR DYSTROPHY

The gastrointestinal tract is colonized by huge number of commensal microorganisms that form the so-called microbiota[44]. In recent years, it was recognized that alterations of gut microbiota (dysbiosis) can cause immune dysregulation, contributing to multitude of diseases of different etiology and DMD patients present alteration of gastrointestinal motility and suffer from constipation, pseudo-obstruction, acute dilatation. Dysbiosis condition could be responsible for the uncontrolled passage of components of the microbiota towards the immune cells of the lamina propria, leading to pathological activation of these cells. Altered intestinal permeability in DMD represents a potential source of metabolites and microbial products, also referred to as pathogen-associated molecule patterns (PAMPs) that could contribute to muscle wasting and activation of the immune system, thus contributing to DMD disease[45,46]. Among the PAMPs, lipopolysaccharides (LPS), a cell membrane component of gram-negative bacteria, is known to interact with the innate sensors like TLR4, resulting in a strong immune response[47]. However, an immune-mediated effect

of microbiota-derived PAMPs in the context of the DMD features has not been considered yet. In addition, microbial dysbiosis interferes with the development of muscle progenitor cells[48], endothelial cell functions[49], as well as the regulatory molecules secreted by skeletal muscle cells and adipose tissues, which are dependent on the production of short-chain fatty acids (SCFAs) and branched-chain amino acids (BCAAs)[50]. Given the progressive deterioration of the alimentary tract's physiology with age, the loss of dystrophin in the gastrointestinal system of individuals with DMD may exacerbate aging-associated inflammation. In line with these hypotheses, we and others demonstrated that age-dependent dysbiosis in 3-month-old mdx mice is associated with alterations in SCFAs, changes in the peripheral and local immune landscape, and compromised muscle integrity[51,52].

ENTERO-THYMIC CIRCUIT

It was assessed that gut microbiota has a strong interplay with the immune system[53] and, in particular, with the unconventional T-cells. These unique cells possess characteristics of both innate and adaptive immune cells and include γδ-T cells (γδ T), invariant natural killer T (iNKT) cells, and mucosa-associated invariant T (MAIT) cells. Unlike conventional B and T cells, unconventional T-cells do not respond to antigens presented by major histocompatibility complex (MHC) molecules. Instead, they recognize signals derived from the microbiota, such as glycolipid antigens (iNKT cells) and microbial vitamin derivatives (MAIT cells). Specifically, MAIT cells are regulated by microbial metabolites derived from vitamins B2 and B9. One such metabolite is 6-hydroxymethyl-8-D-ribityllumazine, which binds to the non-classical MHC class I-like molecule MR1, on thymocytes. This binding influences the expression of pro-inflammatory cytokines such as IFN-γ and IL-17[54]. At barrier sites, MAIT cells determine barrier integrity through close interactions with both innate and adaptive cells of the immune systems. In particular, at early stage of inflammatory events, MAIT cells activate not only dendritic cells (DCs) but also macrophages, effector lymphocytes and memory T-cells. Consistent with these evidences, Ennamorati *et al* showed that early-life microbiota regulates the development and distribution into the thymus of innate lymphocytes (ILCs) expressing the transcription factor PLZF through the migratory plasmacytoid DCs. Intriguingly, MAIT cells abundantly express the PLZF and ILCs are upregulated in DMD, causing the proliferation of eosinophils and overstate inflammation[55].

AIM OF THE STUDY

In this study, we investigated whether healthy and dystrophic aging lead to the proliferation of pathobionts or protective taxa, as well as microorganisms contributing to muscle degeneration and inflammation. Furthermore, we revealed similar altered microbiota richness and metabolism in young and older mdx mice, thereby shedding light on a sustained microbiota dysbiosis during DMD course. Interestingly, microbiota depletion in mdx induced catabolic and autophagic pathways, while coordinating fibrotic and inflammatory signaling negatively in dystrophic muscles. Of note, thymic involution together with increase in peripheral naïve T cell pool and reduced helper and memory activity occurred in microbiota-depleted mdx mice following antibiotics treatment. Since structural integrity of the thymic niche is disrupted in mdx, including disorganization of the cortical and medullary junction[56], we argued that microbiota depletion contributes significantly to accelerate dystrophic thymic involution and reduce the microbial-dependent stimulation of muscle T cells. Overall, this study provide valuable insights into how the intestinal microbiota shapes the inflammatory response, thereby conferring distinct susceptibility to muscle pathology. Furthermore, we potentially identified novel biomarkers associated with gastrointestinal involvement and disease progression prediction, which could be translated into human studies and aid in stratifying patients based on the most appropriate treatments.

MATERIALS AND METHODS

ANIMAL ETHICS STATEMENT

Procedures involving living animals were conformed to Italian law (D.L.vo 116/92) and approved by local ethics committees. This work was authorized by the Ministry of Health and Local University of Milan Committee, authorization number 859/2017-PR (5247B.35, 10/07/2017). C57BL/10 and mdx male mice from Charles River were maintained at the Policlinico Hospital animal facility. All animals were housed in ventilated cages in a 12 h light/dark cycle, with free access to water and standard autoclaved chow. Food intake was measured. No food intake differences were observed between C57BL/10 and mdx mice. For the microbiota depletion experiments, mice were orally gavaged with a mix of antibiotics (ABX) containing vancomycin (1.25 mg), ampicillin (2.5 mg) and metronidazole (1.25 mg) in 200 µl of water for 4 weeks. Animals that eventually suffered from clinical complications during each treatment (enhancement of stress, motor impairments) were excluded from the experimental plan.

GFmdx DERIVATION

We participated at the EC Horizon 2020 funded INFRAFRONTIER2020 project (2017–2020), to obtain mouse axenic service implemented as a Trans-national Access activity. INFRAFRONTIER is the European Research Infrastructure for phenotyping, archiving and distribution of model mammalian genomes by the European Mouse Mutant Archive (EMMA), providing access to tools and data for biomedical research (www.infrafrontier.eu). Through the "INFRAFRONTIER2020 project and microbiome research", in collaboration with the Gnoto/Axenic Facility of the Instituto Gulbenkian de Ciência—partner and founding member of the ECGnoto network http://www.ecgnoto.eu—we generated the GFmdx. Detailed procedure is described below.

STANDARD OPERATIVE PROCEDURE FOR GENERATING GERM-FREE (AXENIC) MICE USING CESAREAN SECTION REDERIVATION

Equipment

- Sterile isolator and set up for rearing germ-free mice.
- Transfer chamber compatible with the isolator.
- Autoclaved water inside the transfer chamber.

Surgical equipment

- Medroxiprogesterone acetate (150 mg/ml, Pfizer).
- VirkonS, 1% solution at room temperature (RT) (Antec Int. Ltd.).

Method

Ensure availability of isolator reared, germ-free surrogate mother with newborn pups (<5 days old) at day 19 of procedure (see below).

Day 2—Set up the relevant mating of foster strain inside the recipient isolator (usually on Sundays).

Day 1—Check for mating plugs inside the isolator and identify the foster females.

Day 0—Check for mating plugs inside the isolator and identify the foster females. If more than two plugs between day 1 and 0, set up the relevant mating of mouse strain to be converted to germ-free status (usually on Wednesdays).

Day 1—Check for mating plugs inside and outside the isolator. Identify the foster and donor female(s) for the experiment.

Day 2—Check for mating plugs inside and outside the isolator. Identify the foster and donor female(s) for the experiment. Separate females from males (if some remain without plug) inside the isolator.

Day 3—Check for mating plugs outside the isolator. Identify the donor female(s) for the experiment. Separate females from males (if some remain without plug), from the strain to be converted to germ-free.

Day 18—Check pregnancies inside and outside the isolators. Give pregnant donor female(s) from day 1, at 17.5 days post coitus (dpc), a subcutaneous injection of medroxiprogesterone acetate (5 mg/0.1 ml).

Day 19—Carefully following the SOP for isolator entry procedures, transfer the sterile instruments and supplies required for surgery into the isolator in which the surrogate female(s) are housed. Prepare the hysterectomy suite/surgical transfer chamber: fill up the reservoir with 1% VirkonS, sterilize the surgical compartment and ventilate it overnight. Give pregnant donor female(s) from day 2, at 17.5 dpc, a subcutaneous injection of medroxiprogesterone acetate (5 mg/0.1 ml).

Day 20—Give pregnant donor female(s) from day 3, at 17.5 dpc, a subcutaneous injection of medroxiprogesterone acetate (5 mg/0.1 ml). Transfer water, paper towels and surgical instruments from the isolator to the sterilized compartment of the transfer chamber. Working in the non-sterile compartment of the surgical transfer chamber or the place where the animals are allocated, sacrifice the donor female by cervical dislocation and submerge the whole animal in the 1% VirkonS

solution for 1 min. Use sterile scissors to open the abdomen. Clamp the top of each uterine horn and the base of the uterus close to the cervix, with mosquito scissors. Cut out the “uterine package,” and place it in the transfer chamber reservoir filled with 1% VirkonS for 1 min. This procedure can be performed for a maximum of two females at the same time. Inside the sterile compartment of the transfer chamber rinse the “uterine package” with sterile water to remove the VirkonS (200 ml of minimal volume of water). On top of a heating pad at 37°C, open the “uterine package” with scissors and take out the pups, taking care do not cut the umbilical cord. After removing the pup from the placenta gently pull the umbilical cord with your forceps. Stimulate breathing of the pups while cleaning them with dry paper towel. When pups are breathing normally and have gained a healthy skin color, transfer them to the isolator housing the foster mother. Gently rub the pups with bedding material from the foster mother's cage. Leave them mixed with the bedding 1 or 2 min. Remove some of the original pups so that the foster mother has the same number of pups to feed. If some pups from the foster mother remain in the cage, mix the adopted ones with them (clean the bedding). Check for adoption not earlier than 24 h after transfer. Monitor a microbiological status of the isolator and the animals it houses 3 weeks after transfer.

Day 21/22—repeat step 20 for pregnant donor females of days 2 and 3, if necessary.

SERUM ANALYSIS

CPK, ALT, AST analyses were performed on serum samples of ABX-treated mdx, GFmdx and untreated mdx mice with CPK/ALT/AST kit (Cobas), according to manufacturer's instructions.

FACS ANALYSIS

Pooled muscle from the leg (QA, TA and gastrocnemius), colonic and splenic tissues of ABX-treated mdx, age-matched mdx and C57BL/10 mice are minced slightly to remove blood trapped vessels and washed in PBS, and then digested at 37°C with 0,2 mg/ml Liberase in DMEM culture medium. Undigested tissues are mashed with a plunger through the filters and washed with DMEM with serum. Then, they are filtered through a 70µm filter, placed on Histopaque 1077 gradient and centrifuged at 400g for 45 min. Cells will be harvested at the interface, washed two times with PBS and then used for flow cytometry analysis. Similarly, murine lamina propria mononuclear cells (LPMC) will be isolated as described in 35. Briefly, the cells are isolated via incubation with 5 mM EDTA at 37°C for 30 min, followed by mechanical disruption with GentleMACS (Miltenyi Biotec). After filtration with 100µm and 70µm nylon strainers (BD), the LPMC are counted and stained for

immunophenotyping. The cells are evaluated for the expression of different immunological subpopulations and multiple-labelled with different groups of antibodies to recognize specific sub-populations (CD45 PerCp, CD4 Pe-Cy7 and Pacific Blue, CD8 efluor 450, CD44 FITC, CD62L PE, CD25 APC, GITR Pe-Cy7, CD3 FITC, Foxp3 Alexa fluor 488, CD11b PE). Murine MAIT cells are identified by gating on the lymphocyte population and excluding doublets using forward/side-scatter properties. At first, we will utilize the MR-1 tetramer that is composed of MR1-5-OP-RU and MR1-6-FP biotinylated monomers in TBS, additionated with 0.5 mg/ml streptavidin-PE, streptavidin-BV421, or unlabeled streptavidin (all from BD Biosciences). This way, 7AAD−CD45+ lymphocytes are gated and further selected as CD19−TCR-β+ while auto-fluorescent cells are excluded according to BV525 and BV585 fluorescent channels. In the end, we will isolate TCR-β+MR1-5-OP-RU tetramer+ MAIT. To isolate γδ T-cells, we will employ TCRγδ-eBioGL3-PE while – for the NKTs – CD49b-APC, and NKp46-PE or NK1.1-PE. Alternatively unloaded and α-GalCer analogue (PBS-57)-loaded CD1d tetramers will be provided by Thermofisher and used for iNKT cell detection (1.2µg for 106 cells in 100µl), together with anti-mouse TCRβ antibody (REA318; Miltenyi Biotec). In a second step, to assess the cytokines produced or pro-inflammatory mediators expressed by ITC, we can analyze mdx-derived ITC cells for the expression of IFNγ-PE-Cy7; IL-17-PE; T-bet-PE-Cy7; RORγt-APC (all from eBioscience) by means FACS. We will grossly isolate DCs for the expression of CD45, CD11c and MHC-II and then follow the expression of CD317, Siglec-H, CD45R and Ly-6C for the plasmacytoid DCS (pDCs); CD8a, XCR1, CD24 and CLEC9A for conventional DC1 (cDC1); CD4, SIRP□ and CD11b for conventional DC2 (cDC2). Tissues will be depleted from fat and connective tissue, transferred to 6-well plate containing Liberase (Invitrogen) solution and incubated at 37 °C for 20 min. Following dissociation, we will identify the main thymic cellular subpopulations according to the combined expression of CD4 (Pacific Blue-A) and CD8 (APC-Cy7-A). CD4+/CD8+ double positive cells will be subsequently characterized for the expression of CD69 (AF 488-A) and TCR□ (PE-A); the double-negative cells for the expression of CD44 (AF 488-A) and CD25 (APC-A); the CD4+ subpopulation for Foxp3 (AF 488-A) and CD25 (APC-A) to identify the T-regs. For FACS characterization, data are acquired with the BD Canto II machine and analyzed with FlowJo 9 software. Each analysis includes at least 105 events for each gate.

HISTOLOGICAL ANALYSIS MICROBIOTA ANALYSIS

TA muscle tissues were collected from ABX-treated mdx, GFmdx, untreated mdx and C57BL/10 mice, frozen in liquid-nitrogen cooled isopentane and cut on a cryostat into 10µm. Gömöri

trichrome staining was performed to evaluate the morphology and the percentage of fibrosis. Adjacent sections were stained with H&E. Frozen sections were brought to RT and placed in preheated Bouin's fluid (BF) at 56°C for 15 min. Equal volumes of Hematoxylin Weigert's Iron Part A and B (Bio-Optica, Milan S.p.A. Italy) were applied to tissue sections for 5 min. Then, acid alcohol solution (0.5%) was applied to sections for 10 s, to stain cytoplasm, followed by Acid Fuchsin solution (Bio-Optica, Milan S.p.A. Italy) diluted 1:2 in deionized water for 5 min. Tissue sections were incubated with phosphomolybdic acid (Bio-Optica, Milan S.p.A. Italy) for 5 min to block the staining of all tissue components other than connective tissue fibers. Then, slides were incubated with Aniline Blue solution (Bio-Optica, Milan S.p.A., Italy) for 5 min to stain collagen fibers. Finally, slides were washed in deionized water combined with 1% glacial acetic acid (Carlo Erba, Milan, Italy) and incubated for 30 s in 100% ethanol solution, for dehydration. 100% Xylene (Sigma-Aldrich, USA) for 1 min before mounting with DPX reagent (VWR International, USA) and coverslips. Frozen sections were characterized by immunofluorescence staining. Slides were fixed with 4% paraformaldehyde for 10 min, permeabilized with 0.3% Triton X-100 for 15 min and incubated with 10% donkey serum to block non-specific binding for 1 h and then incubated with the primary antibodies (overnight at 4°C) diluted in blocking solution. Fluorochrome-conjugated secondary antibodies were diluted in PBS and added for 1h at RT. Primary antibodies were used at the following dilutions: fibers type I 1:50 (BA-D5, Developmental Studies Hybridoma Bank, Douglas Houston); fiber type IIA 1:50 (sc-71, Developmental Studies Hybridoma Bank); fiber type IIB 1:50 (BF-F3, Developmental Studies Hybridoma Bank). Slides were then mounted with Prolong Gold® Antifade Reagent with DAPI (Thermo Fisher, Carlsbad, CA). Leica Dmi8 fluorescence microscope was used for acquiring images. Histological identification of slow/type I, fast fatigue resistant/type IIa, and fast fatigable/type IIb fibers was performed by staining for either myosin ATPases or oxidative enzyme capacity (succinate dehydrogenase, SDH). Enzymatic activity of SDH was assayed by placing the slides in SDH incubating solution, containing sodium succinate as a substrate and nitro-blue tetrazolium (NBT) for visualization of reaction for 1 h at 37°C. At first, slides were incubated for 10 s in 30–60–90–60–30% acetone solution and, then, for 30 s in 80–90–100% ethanol solution for dehydration. Finally, 100% Xylene (Sigma-Aldrich, USA) for 1 min before mounting with DPX reagent (VWR International, USA) and coverslips. For Gömöri trichrome and SDH staining, images were captured by Leica microdissector (CTR6000).

WESTERN BLOT ANALYSIS

Tibialis anterior skeletal muscles and colonic tissues were isolated from ABX-treated mdx, GFmdx, and age-matched untreated mdx or C57Bl mice and total proteins were obtained as in[57]. Samples were resolved on polyacrylamide gels (ranging from 6 to 14%) and transferred to nitrocellulose membranes (Bio-Rad Laboratories, California, USA). Filters were incubated overnight with following antibodies: LC3B (1:500, L7543, Sigma-Aldrich); TGFβ (1:500, e-ab-33090, Elabscience); NF-kB (1:500, sc-514451, Santa Cruz Biotechnology – SCB); RELb (1:500, sc-48366, SCB); FKHR-FOXO1 (1:500, sc-374427, SCB); TLR4 (1:500, sc-293072, SCB); vinculin (1:500, MA5-11690, Invitrogen); TOMM20 (1:500, AB186735, Abcam); DRP1 (1:500, AB184247, Abcam); P62 (1:500, P0067, Sigma-Aldrich); COX IV (1:500, AB16056, Abcam); AKT 1-2-3 (1:500, ab179463, Abcam); PPARγ (1:500, AB59256, Abcam); HDAC1 (1:500, MA5-1807, Invitrogen); HDAC2 (1:500, 51-5100, Invitrogen); ATG7 (1:500, PA5-35203, Thermofisher Scientific); PKCα (1:500, ab32376, Abcam); AMPKα (1:500, sc74461, SCB); Atrogin (1:500, ab168372, Abcam); Murf-1 (1:500, PA5-76695, Invitrogen); p-4EBP1 (1:500, 9451, Cell Signaling Technology); 4EBP1 (1:500, 9644, Cell Signaling Technology); S6RB (1:500, 2217, Cell Signaling Technology); Filters were detected with peroxidase conjugated secondary antibodies (Agilent Technologies, California, USA) and developed by ECL (Amersham Biosciences, UK).

MICROBIOTA ANALYSIS

We performed DNA extraction, 16S rRNA gene amplification, purification, library preparation and pair-end sequencing on the Illumina MiSeq platform as previously described in[58]. MICCA pipeline (v.1.7.0) (http://www.micca.org) was used to pre-process the reads[59] while micca trim and micca filter were employed for forward/reverse primers trimming and quality filtering, respectively. Filtered sequences were denoised using the UNOISE algorithm implemented in micca otu to determine true biological sequences at the single nucleotide resolution by generating amplicon sequence variants (ASVs). Micca classify and the Ribosomal Database Project (RDP) Classifier v2.11 were used to classify taxonomically the bacterial ASVs[60] while Nearest Alignment Space Termination (NAST) algorithm performed the multiple sequence alignment (MSA) of 16S sequences[61] as described in detail in[62] (release 13_08). Phylogenetic trees were inferred using micca tree[63]. Indeed, we reduced sampling heterogeneity rarefying samples at the depth of the less abundant sample using micca tablerare while we performed the phyloseq R package to assess alpha (within-sample richness) and beta- diversity (between-sample dissimilarity)[64]. P-values were False Discovery Rate corrected using the Benjamini-Hochberg procedure implemented in DESeq2

and the R package DESeq2 was used to test differential abundance[65]. The psych R package was used to compute Spearman's correlation tests. Prediction of functional metagenomic content was inferred by using Piphillin[66] with the reference curated databases BioCyc[67] and Kyoto Encyclopedia of Genes and Genomes (KEGG)[68]. iPATH 3 was used to construct the metabolic pathway (https://pathways.embl.de/).

METABOLOME ANALYSIS

To extract the metabolome from the GI tissues of ABX-treated and age-matched untreated mdx or C57Bl mice we used the the MetaboPrep kit (Theoreo, Montecorvino Pugliano, SA) as in[69,70] according to manufacturers' protocol. Analysis was conducted in gas-chromatography coupled with mass spectrometry (GC-2010 Plus gas chromatograph and 2010 Plus single quadrupole mass spectrometer; Shimadzu Corp., Kyoto, Japan). Chromatographic separation was achieved as previously reported using a 30 m 0.25 mm CP-Sil 8 CB fused silica capillary GC column with 1.00 µm film thickness from Agilent (J&W Scientific, Folsom, CA, USA), with helium as carrier gas. Untargeted metabolites were identified by comparing the mass spectrum of each peak with the NIST library collection (NIST, Gaithersburg, MD, USA). To identify metabolites, the linear index difference max tolerance was set at 50, while the minimum matching for the NIST library search was set at 85%. According to MSI level 1 standard[71], the relevant putative metabolites was further confirmed using an independent analytical standard analysis. The normalization procedures consisted of data transformation and scaling. Statistical analyses were conducted on transformed (og transformation) and autoscaled (mean-centered and divided by the standard deviation of each variable) data. Partial least square discriminant analysis (PLS-DA) was performed on internal standard peak area normalized chromatogram using R. Classification and cross-validation were performed using the wrapper function included in the caret package. A permutation test was performed to assess the significance of class discrimination. Variable importance in projection (VIP) scores were calculated for each component. For each relevant metabolite, the Mouse Metabolome Database ID number was determined. Metabolic pathways associated with these metabolites were analyzed using the MetScape application[72]. Metabolic pathways involvement was also evaluated using the MetPa tool[73].

RNASEQ ANALYSIS

Library Preparation and DNA Sequencing: 150–300 ng of total RNA determined by InvitrogenTM QubitTM high-sensitivity spectrofluorometric measurement was poly-A selected and reverse

transcribed using Illumina's TruSeq stranded mRNA library preparation kit. Each sample was fitted with one of 96 adapters containing a different 8-base molecular barcode for high-level multiplexing. After 15 cycles of PCR amplification, completed libraries were sequenced on an Illumina NovaSeqTM 6000, generating 20 million or more high-quality, 100-base, long-paired end reads per sample. RNA-Seq Analysis: A quality control check on the fastq files was performed using FastQC. Upon passing basic quality metrics, the reads were trimmed to remove adapters and low-quality reads using default parameters in Trimmomatic1[74]. Alignment, Transcript Abundance and Differential Gene Expression Analysis: The trimmed reads were then mapped to a reference genome using default parameters with strandness (R for single-end and RF for paired-end) option in Hisat22[75]. In the next step, transcript/gene abundance was determined using kallisto3[76]. We first created a transcriptome index in kallisto using Ensembl cDNA sequences for the reference genome. This index was then used to quantify transcript abundance in raw counts and transcript per million. Fold-changes between groups were calculated using EdgeR from the Bioconductor package[77]. PCA on differentially expressed genes was performed using ClustVis[78]. Gene ontology (GO) analysis was conducted submitting gene lists to the PANTHER Enrichment Test (release 16.0), built-in analytical tool in the AmiGO2 software suite by the GO consortium[79]. GO analyses were conducted on the GO database (version 2021-05-01), using all genes in the Mus musculus database as reference list and the GO Biological Process Complete as annotation dataset. Significantly enriched GO terms were identified by adjusted P-value<0.05. GSEA was performed via dedicated software (release 4.2.3) by Molecular Signatures Database (MSigDB). The “Hallmark” annotated gene set collection was used for analysis of ranked gene lists.

IMAGE QUANTIFICATION

Histological images were captured by Leica microdissector, fluorescent microscope and confocal microscopy. Quantitative analyses were performed by ImageJ Software (NIH). Threshold color Plug in of ImageJ Software was used to quantify the Gömöri trichrome staining as percentage of area over a fixed grid area. For IF quantification, confocal acquisition of n = 12 muscle cross-sections for distinct TA muscles were obtained from each experimental animal used for each protocol. Data were analyzed by GraphPad Prism and expressed as means±SD.

STATISTICS

To determine the significance of the variation of cellular concentration throughout the time, we used the linear regression for repeated measures. To compare multiple-group means, one-way

ANOVA followed by Tukey's multiple-comparison test or non-parametric test followed by Kruskal–Wallis test were used to determine significance (*P<0.05, **P<0.01, ***P<0.001; ****P<0.0001). To compare two groups, Student's t-test was applied assuming equal variances (*P<0.05, **P<0.01, ***P<0.001; ****P<0.0001). Sample size was determined by using a sample-size calculator freely available on internet. All the samples that did not rich quality control standards due to the presence of contaminants for RNA or to problems in freezing procedures for histological analysis were excluded. The analysis of Alpha diversity index to evaluate microbiota richness was based on Wilcoxon rank-sum test on row data.

RESULTS

AGE-RELATED DYSBIOSIS IN mdx

To evaluate the impact of aging on the intestinal microbial community of mdx and C57Bl mice, we conducted a metataxonomic analysis comparing 3 and 9-month-old (respectively, 3m and 9m) animals. This comprehensive analysis of the gut microbiota revealed reduced enrichment of amplicon sequence variants (ASV) in mdx mice of both age groups compared to age-matched wild type C57Bl mice, confirming the presence of dysbiosis in dystrophic animals. Furthermore, we observed that the differences in microbiota composition between aged mice were less pronounced compared to younger mice, indicating that aging affects microbiota richness even in healthy conditions (Fig. 1A). Principal Coordinates Analysis (PCoA) demonstrated the distinct separation of healthy and dystrophic mice, emphasizing both individual and group dissimilarities (Fig. 1B) that we further elucidated employing linear discriminant analysis Effect Size (LEfSe) to examine the biological consistency of divergent organisms[80]. We found that Helicobacter, Firmicutes, and Clostridium were abundant in 9m C57Bl mice, while Bacteroides, Prevotella, and Odoribacter were upregulated in age-matched mdx mice (Fig. 1C). When comparing the microbiota content of C57Bl and mdx mice across different ages, we identified Prevotella, Alistipes, Anaeroplasma, and Odoribacter as common signatures in mice with Duchenne muscular dystrophy (DMD) (Fig. 1D), consistent with previous findings9. Additionally, comparing 3m and 9m mice, we observed an upregulation of Akkermansia and Lactobacillus in younger C57Bl mice, whereas Helicobacter and Alistipes were more abundant in 3-month-old mdx mice (Fig. 1E).

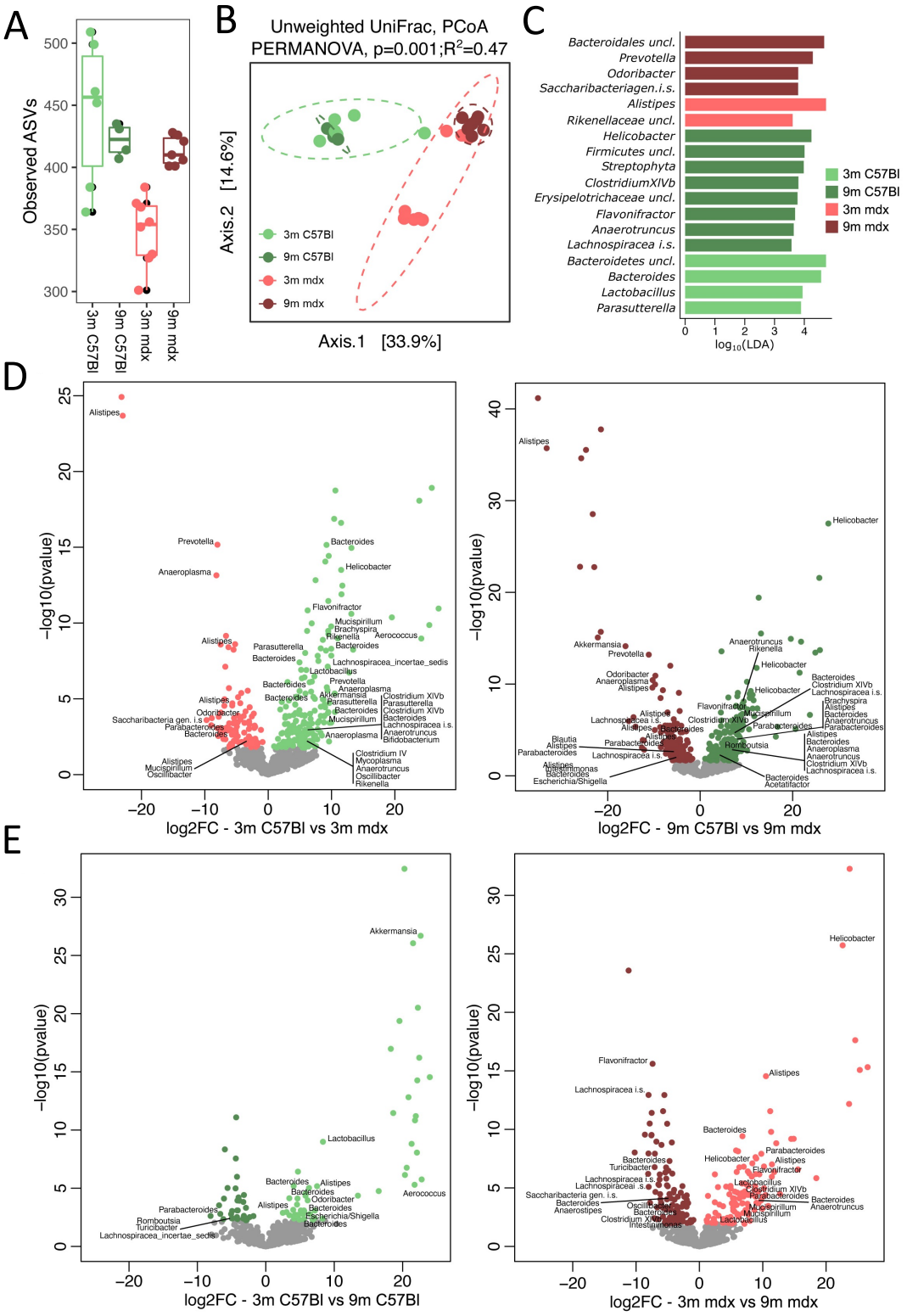

Figure 1. ***Microbiota dysbiosis is a common feature of 3m mdx and 9m mdx mice***

(a) Observed number of enriched ASVs in 3m C57Bl, 3m mdx, 9m C57Bl and 9m mdx (n=5 each). (b) Unweighted UniFrac PCoA of 3m C57Bl, 3m mdx, 9m C57Bl and 9m mdx (n=5 each). (c) LEfSe Analysis among groups. Enrichment of specific

micro-organisms according to the pathology – 3m C57Bl vs 3m mdx and 9m C57Bl vs 9m mdx – (d) and to the age – 3m C57Bl vs 9m C57Bl and 3m mdx vs 9m mdx (e).

Consistent with the findings, the predicted functional potential of the microbiota associated with mdx mice and aging revealed notable alterations in metabolic pathways (Fig. 2A, B). Specifically, 9m mdx mice exhibited upregulation in pathways related to the biosynthesis of amino acids (tyrosine and tryptophan), lysine, and fatty acids. Additionally, they displayed changes in the metabolism of various molecules including histidine, nitrogen, riboflavin, and glycerophospholipids. In contrast, age-matched C57Bl mice showed upregulation in glutathione, glyoxylate, and dicarboxylate metabolism. Furthermore, in the analysis of 3m mdx mice, we identified an overactive glycolysis and gluconeogenesis, glycerol lipid metabolism, and biosynthesis of unsaturated fatty acids (Fig. 2A, B). Given the slight differences observed previously in 3-month-old mice, we examined the levels of SCFAs in aged animals. We discovered a significant downregulation of SCFAs, particularly butyric acid, acetic acid, and propionic acid, in 9m mdx mice compared to age-matched controls. Additionally, isobutyric acid levels increased, while isovaleric acid was not detectable in dystrophic mice (Fig. 2C). Intriguingly, we also investigated whether aging had an impact on SCFAs content. We found an upregulation of total SCFAs, particularly acetic acid and propionic acid, in 9m C57Bl mice compared to 3m C57Bl mice. However, the only discernible difference in the dystrophic background was related to butyric acid (Fig. 2C).

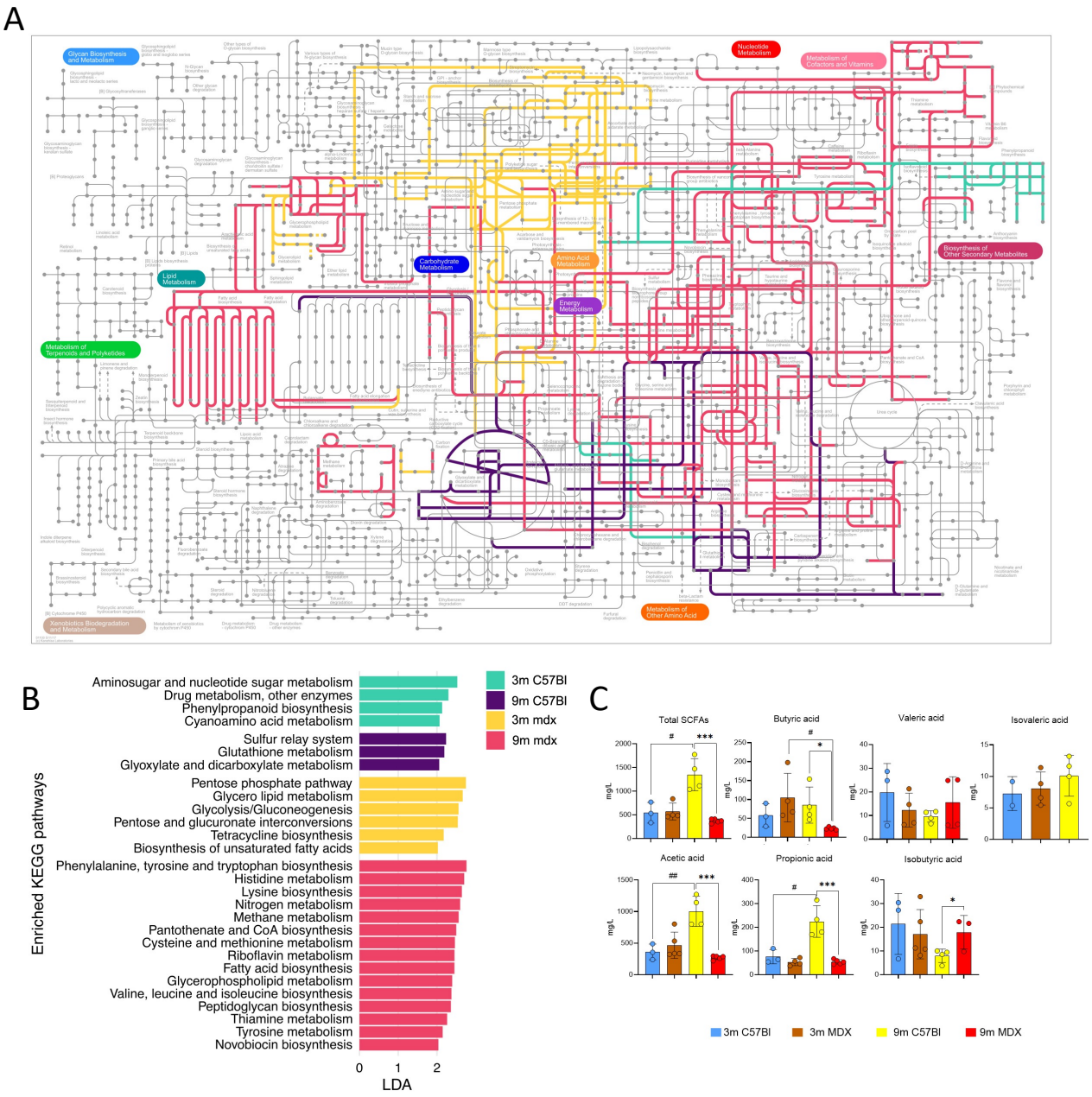

Figure 2. ***KEGG metabolic pathways and SCFAs content in 3 months-old and 9 months-old healthy and dystrophic mice***

(a) The iPath3.0 representation of KEGG metabolic pathways inferred from Piphillin analysis significantly upregulated (in red) or downregulated (in blue) in 3m C57Bl, 3m mdx, 9m C57Bl and 9m mdx (n=5 each). Nodes in the map coloured in green, yellow, and orange correspond to acetate, propionate, and butyrate, respectively. Line thickness represents the level of statistical significance for the inferred pathways; thick lines with FDR-corrected p-value<0.05, thin lines with nominal p-value <0.05. (b) Enriched KEGG pathways representation in 3m C57Bl, 3m mdx, 9m C57Bl and 9m mdx (n=5 each). (c) SCFA faecal quantification of 3m C57Bl, 3m mdx, 9m C57Bl and 9m mdx (n=5 each).

Recognizing the crucial role of the metabolome in determining host-microbe interactions and immune system development, we conducted a metabolomic analysis of the small intestine in aged mice (Fig. 3A, B) and reconstructed pathways using metabolites with the highest discriminatory power. In the small intestine of 9m mdx mice, we observed an overexpression of propylene glycol, ethanolamine, and simple sugars (lactose and maltose), while myo-inositol, glucose, and uridine were downregulated. Myo-inositol is known to be involved in lipid signaling, glucose metabolism, and insulin regulation, while glucose and uridine play roles in glucose balance as well as lipid and amino acid metabolism[81,82]. Conversely, age-matched C57Bl mice exhibited upregulation of myo-inositol, glucose, and uridine (Fig. 3B). Consistent with these findings, we determined that the most enriched sets of metabolites were associated with antibiotics biosynthesis, galactose metabolism, sucrose metabolism, and lipid metabolism (Fig. 3C). To assess whether aging significantly affected the modulation of metabolites previously reported in the intestines of younger mice[83], we re-analyzed the data. We found that 3m and 9m C57Bl mice both exhibited overexpression of metabolites involved in simple sugar metabolism such as glucose, ribose, galactose, and phenylalanine. Additionally, dystrophic mice showed upregulation of 3-phenyllactic acid (Fig. 3D, E). Interestingly, the metabolome of 9m C57Bl mice was distinct from that of all other animals (Fig. 3E). Finally, we determined that the most enriched sets of metabolites were associated with galactose metabolism, sucrose metabolism, fructose metabolism, and amino acid biosynthesis (tyrosine, phenylalanine, tryptophan, arginine) (Fig. 3F).

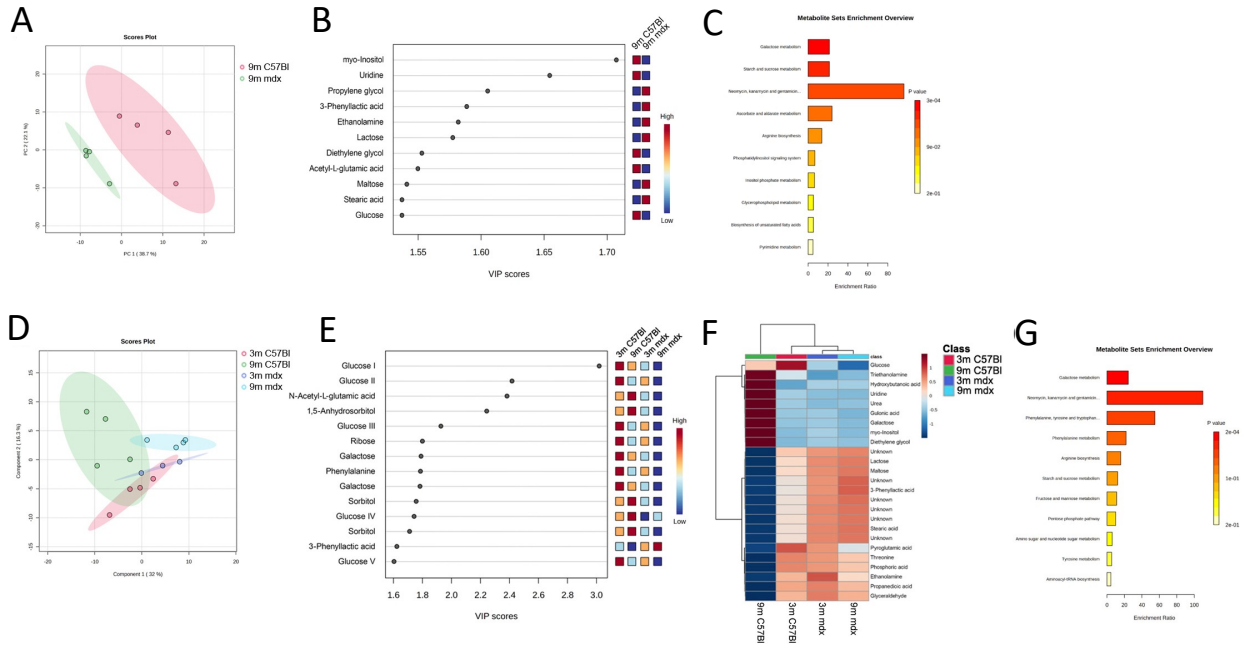

Figure 3. ***Metabolome variations in intestinal samples of 3 months-old and 9 months-old healthy and dystrophic mice***

(a) Partial Least Square Discriminant Analysis (PLS-DA) score plot of 9m C57Bl and mdx (n=4 each) gut tissue samples. (b) Concentration of the metabolites with a variable importance in projection (VIP) score higher than 1.5 isolated from the small intestinal content and the heatmap of the concentration of the top 10 metabolites according to ANOVA. The metabolites in blue have a negative fold change while those in red have a positive fold change. (c) Overview of the enriched metabolite sets. (d) PLS-DA score plot of 3m C57Bl, 3m mdx, 9m C57Bl and 9m mdx (n=4 each) gut tissue samples. (e) Concentration of the metabolites with a VIP score higher than 1.6 isolated from the small intestinal content and the relative heatmap of the concentration of the top 14 metabolites according to ANOVA. (f) Heatmap showing all the relevant metabolites concentration change among the 4 groups. Both metabolites and classes were clusterized according to the Wald method. (g) Overview of the enriched metabolite sets.

UNCONVENTIONAL T CELLS MODULATION IN DYSBIOTIC mdx MICE

To correlate how our data concerning the differences in microbiota and SCFAs could impact on muscular phenotype in mice according to dystrophic background and aging and how these variables could influence the sustained activation of the innate immune response of mdx mice[84], we took into consideration conventional and unconventional T-cells abundancy in tissues normally affected by dystrophin deficiency (skeletal muscle) and organs that are the well-recognized sites for inflammatory responses (colon, thymus and spleen). MAIT are activated by the riboflavin 35, whose metabolism is upregulated in 9m mdx metabolic pathways (Fig. 2B) and SCFAs could alter the antimicrobial activity of MAIT or the pro-inflammatory switch of iNKT 36, paving the way for additional regulation of these cell according to aging and pathology (Fig. 2C). In the spleen of 9m C57Bl we found an upregulation of CD3+ cells, while their abundance diminished according to aging in mdx mice (Fig. 4A). As the subpopulations of CD4+ T-cells did not change significantly (Fig. 4B), we assessed notable upregulation of CD8+ T-cells in 9m C57Bl according to 3m C57Bl and age-matched mdx mice while – as expected – CD8+ inflammatory subpopulations (as those expressing CD69+, IFN-γ, IL-17) were upregulated in dystrophic mice and slightly diminished according to the age (Fig. 4C). In last analysis, bone-marrow derived circulating CD45+CD11+ myeloid cells were over-expressed in 9m mdx related to 3m mdx mice while in C57Bl we found an opposite situation (Fig. 4D). iNKT cells were dramatically upregulated in 9m mdx mice compared to 3m mdx mice and age-matched C57Bl mice, as were the IFN-γ+ iNKT cells (Fig. 4E). Accordingly, infiltrating CD69+ and activated IFN-γ+/IL-17+ subpopulations of MAIT were significantly increased in spleen of older mdx compared to age-matched C57Bl mice (Fig. 4F). These data suggest a possible correlation between increased riboflavin and activation of spleen-derived MAIT and iNKT cells 14 in older mdx.

In last analysis γδ T-cells were up-regulated in dystrophic mice related to age-matched controls: significant differences were assessed in those expressing IL-17 (Fig. 4G).

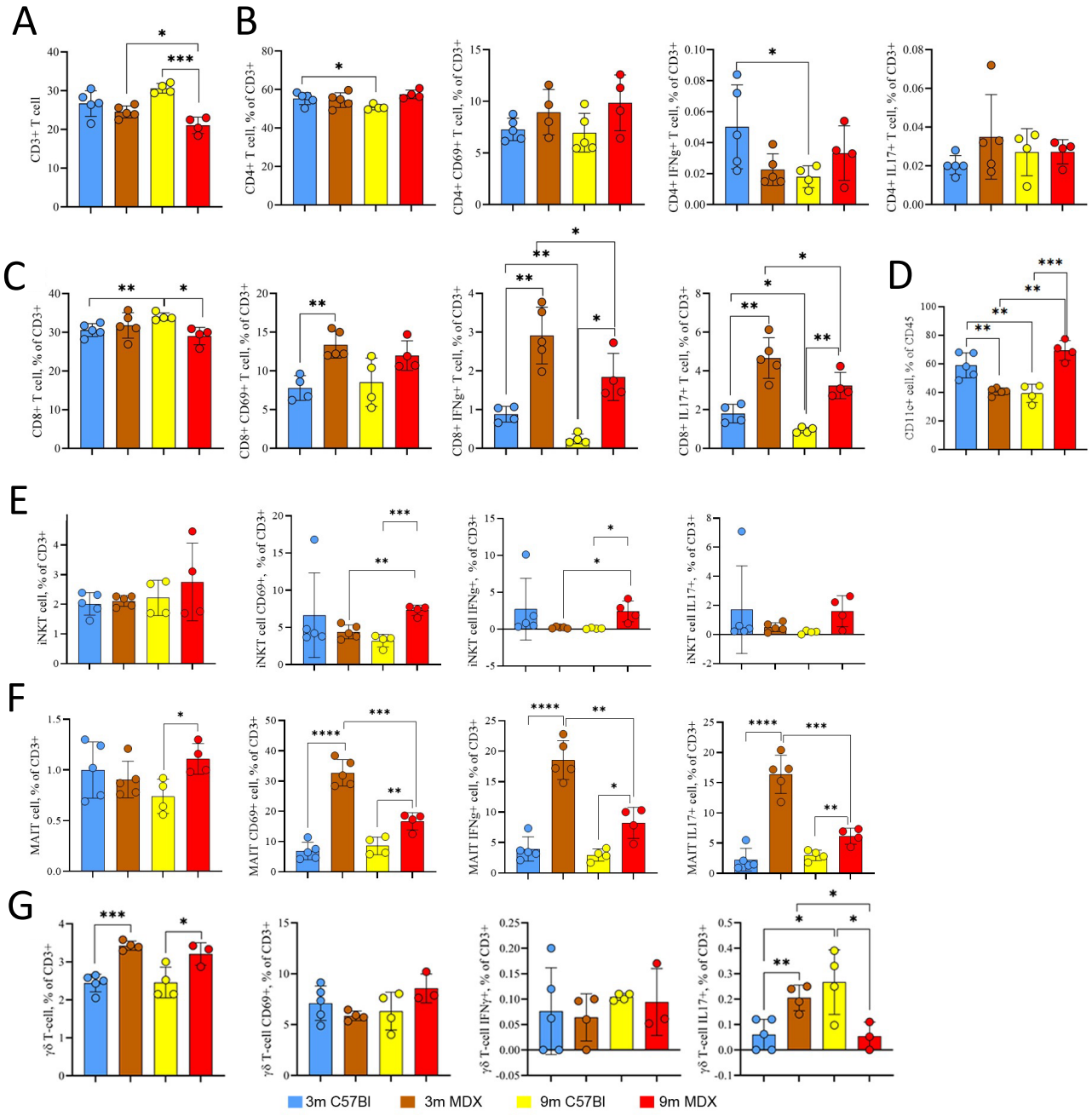

Figure 4. ***Splenic conventional and unconventional T-cells evaluation in 3m and 9m mdx mice***

FACS analysis of immune cells from spleen of 3m C57Bl (n=5), 3m mdx (n=5), 9m C57Bl (n=4) and 9m mdx (n=4). Graphs show cumulative frequencies of conventional CD3+ T cells (a); CD4+ T-cells and subpopulations expressing CD69, IFN-γ and IL17 (b); CD8+ T-cells and subpopulations expressing CD69, IFN-γ and IL17 (c); CD45+CD11c+ myeloid cells (d).

Graphs show cumulative frequencies of unconventional CD3+ iNKT (e), MAIT (f) and γδ (g) T-cells expressing CD69+, IFN-γ+ and IL17+ markers.

*Data information: data are presented as mean ± SD (*p<0.05; **p<0.01; ***p<0.001; ****p<0.0001; Student t-Test with Welch's correction).*

Colonic CD3+ T-cells were up-regulated in 3m mdx related to age-matched C57Bl and 9m mdx mice (Fig. 5A), while activated CD4+ subpopulations were increased in 3m C57Bl according to pathology and the age (Fig. 5B). CD8+ T-cells were over-expressed in 3m mdx related to 3m C57Bl and in 9m C57Bl related to younger ones: in particular, the CD8+CD69+ cells were increased in 9m C57Bl while CD8+IFNγ+ in 9m mdx (Fig. 5C). CD45+CD11+ myeloid cells were over-expressed in 3m mdx and 9m C57Bl mice (Fig. 5D). The number of iNKT and MAIT cells in the colon of older C57Bl and mdx mice was decrease compared to younger ones (Fig. 5E). Additionally, activated CD69+ iNKT cells and pro-inflammatory IFN-γ+ iNKT cells were downregulated in aged mdx mice (Fig. 5F). γδ T-cells expressing CD69+ were over-expressed in 3m C57Bl while those expressing IFN-γ+ in 9m mdx (Fig. 5G). This age-related decline in the frequency of MAIT and iNKT cells has been previously described in both human and mice 15 and might correlate to the reduced amounts of SCFA in the colon (Fig. 2C).

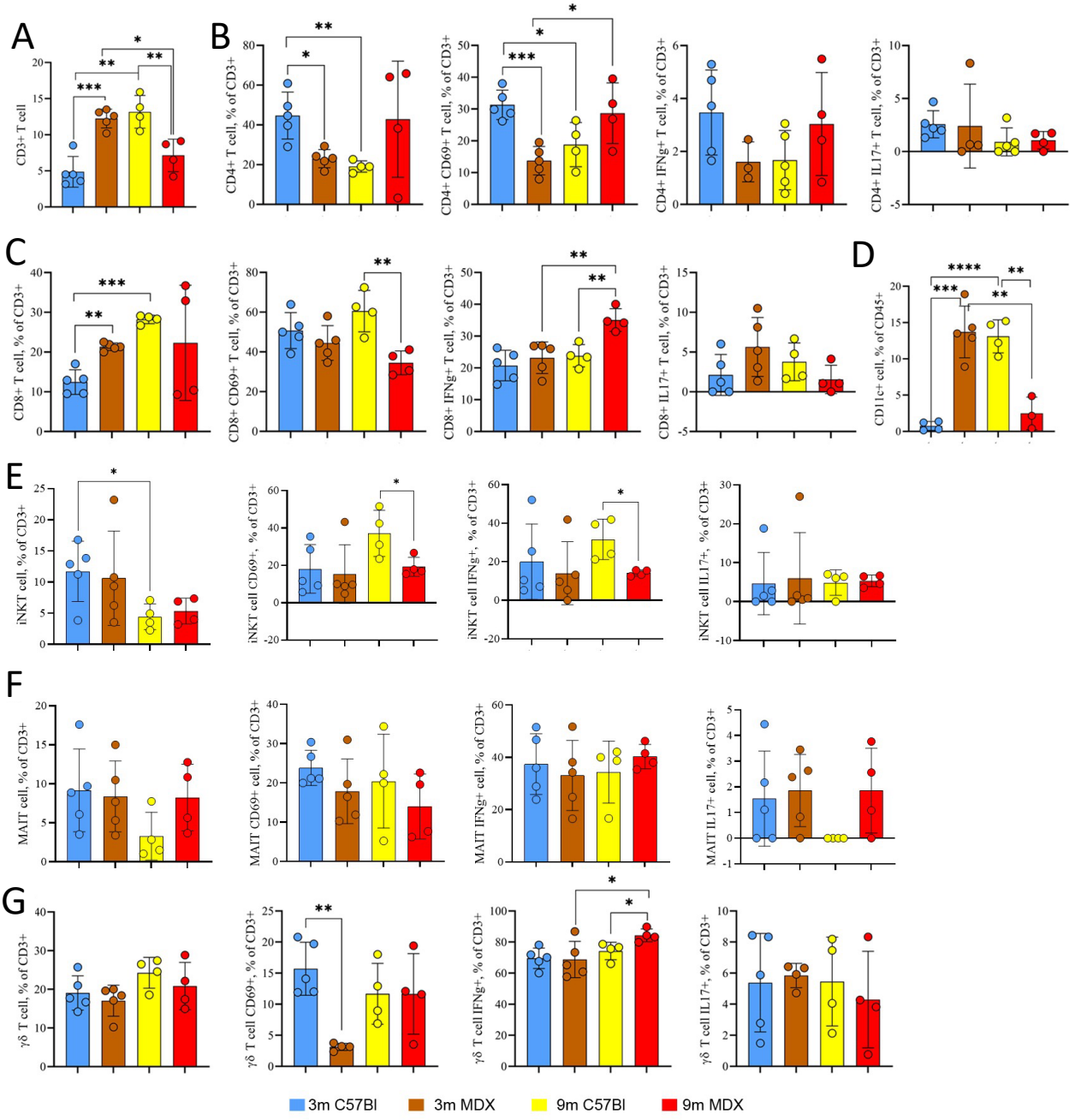

Figure 5. ***Colonic conventional and unconventional T-cells evaluation in 3m and 9m mdx mice***

FACS analysis of immune cells from colon of 3m C57Bl (n=5), 3m mdx (n=5), 9m C57Bl (n=4) and 9m mdx (n=4). Graphs show cumulative frequencies of conventional CD3+ T cells (a); CD4+ T-cells and subpopulations expressing CD69, IFN-γ and IL17 (b); CD8+ T-cells and subpopulations expressing CD69, IFN-γ and IL17 (c); CD45+CD11c+ myeloid cells (d). Graphs show cumulative frequencies of unconventional CD3+ iNKT (e), MAIT (f) and (g) γδ T-cells expressing CD69+, IFN-γ + and IL17+ markers.

*Data information: data are presented as mean ± SD (*p<0.05; **p<0.01; ***p<0.001; ****p<0.0001; Student t-Test with Welch's correction).*

According to the inflammatory background of 3m mdx mice, we found in the hindlimb muscles of these mice that CD4+ T-cells were over-expressed as well as CD4+CD69+ T-cells (Suppl. Fig. 1A, B). Similarly, dystrophic mice up-regulated the CD8+ cells (Suppl. Fig. 1C). CD45+CD11+ myeloid cells were barely detectable in 9m C57Bl and were more abundant in 3m and 9m mdx mice (Suppl. Fig. 1D). As expected, due to the low abundance of these cells in skeletal muscles, we did not observe significant modulation of iNKT and MAIT cells in limb muscles (Suppl. Fig. 1E,F) while γδ T-cells and CD69+ γδ T-cells were drastically over-expressed in dystrophic mice (Suppl. Fig. 1G).

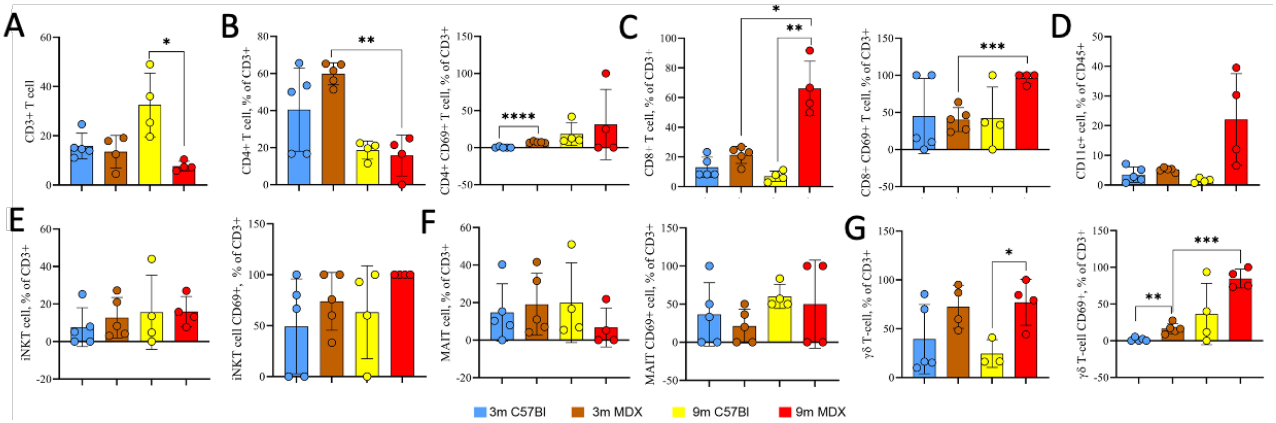

Suppl. Fig. 1. ***Muscular evaluation of conventional and unconventional cells in 3m and 9m mdx mice***

FACS analysis of immune cells from hindlimb muscles of 3m C57Bl (n=5), 3m mdx (n=5), 9m C57Bl (n=4) and 9m mdx (n=4). Graphs show cumulative frequencies of conventional CD3+ T cells (a); CD4+ T-cells and CD4+CD69+ T-cells (b); CD8+T-cells and CD8+CD69+ T-cells (c); CD45+CD11c+ myeloid cells (d). Graphs show cumulative frequencies of unconventional of total and CD69+ CD3+ iNKT (e), MAIT (f) and (g) γδ T-cells.

*Data information: data are presented as mean ± SD (*p<0.05; **p<0.01; ***p<0.001; ****p<0.0001; Student t-Test with Welch's correction).*

THYMIC INVOLUTION IS DEPICTED IN AGED mdx MICE

Thymic involution is an age-related decline in organelle size and function, and it is normally accompanied to diminished cellularity as mTEC and cTEC; disruption of stromal microenvironment that is evident in negative modulation of the cortical-medullary junction and perivascular space[85]. All these events determine drastic down-regulation of immune functions as the accumulation of specific dysregulated CD4 T-cell subsets (as the memory T-cells in place of naïve ones) and, as opposite, the development of autoimmune phenomena. Following these premises, we evaluated these aspects in thymi obtained from 9mo mdx mice in comparison to younger ones.

In the thymus, interactions with both cortical and medullary microenvironments determine the development of self-tolerant conventional CD4+ and CD8+ αβT cells. Indeed, the cortex is fundamental for guiding the proliferation of iNKT cells and it is the necessary to regulate innate and adaptive immune responses. Interestingly, we determined that in 3m mice there was a down-regulation of medullary/cortex ratio in mdx mice while, in opposite, there was an upregulation in older mdx mice related to age-matched C57Bl. Indeed, we found that aging in C57Bl determined a down-regulation of medullary/cortex ratio while in mdx we described an upregulation of this value, suggesting a significant long-term effects on T-cells (Fig. 6A,E). In general, we showed that the larger medulla zone in 3m C57Bl is scattered and faintly defined in the cortico-medullary junction in mdx; thus, aging determined dysfunctions in the organization of thymic architecture, leading to formation of medullary islands (Fig. 6A). In the thymic medulla, it is well described the presence of the myoid cell, that share a structure closely related to that of the muscle as express MyoD, AChR and muscle creatine kinase and are regulated by myogenin and myf5[86]. Since myoid cells are responsible for enhancing the autoimmune response in myasthenia gravis (MG), it was proposed a role in DMD in the regulation of autoimmunity and tolerance induction, as well as in the selection during of mature and immunocompetent T-lymphocytes. This way, we performed immunofluorescence staining for the expression of MyoD+ cells in thymus and we found that these cells were more abundant in 3m C57Bl mice related to 9m C57Bl and 3m mdx mice, in accordance with data published by. Intriguingly, we found that the MyoD+ cells in 9m mdx mice were comparable to those of younger ones (Fig. 6B,D). Indeed, we calculated the vascularized area according to medulla/cortex ratio and we assessed no modulations in control mice and significant down-regulation in 9m mdx mice (Fig. 6D). Dendritic cells (DCs) in the thymus are involved mainly in central tolerance formation, but also in pathogen recognition. We performed immunofluorescence on thymic tissues to evaluate the presence CD11c+CD11b+ DCs and we found that aging determined a down-regulation of these cells in C57Bl mice while it caused an over-expression in dystrophic thymi. Intriguingly, we found that in age-matched thymi there was an upregulation of DCs in 3m C57Bl mice while we found a diminished expression in 9m C57Bl related to mdx mice (Fig. 6E), suggesting modulatory effects on autoreactive thymocyte screening.

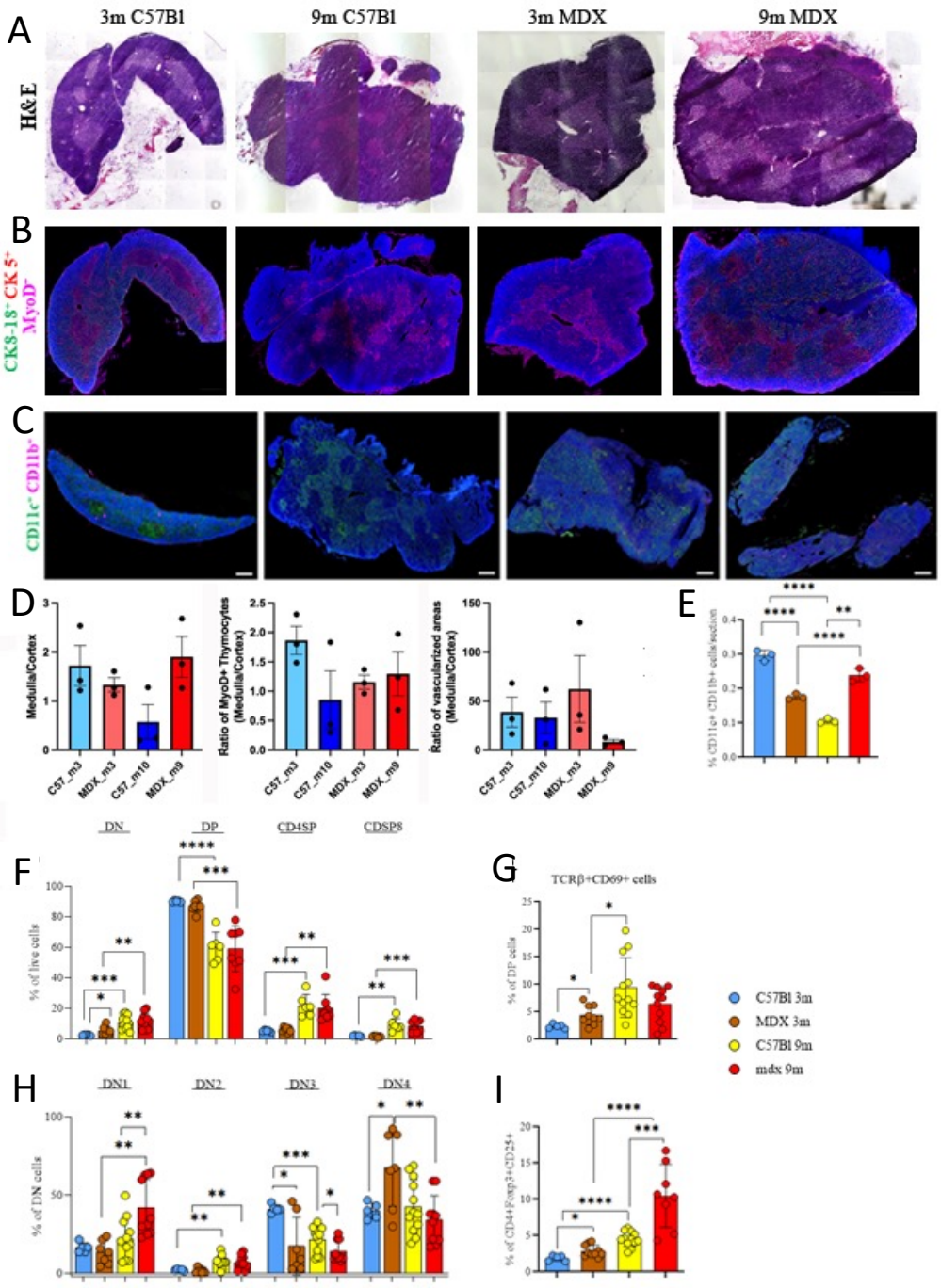

Figure 6. ***Thymus morphology and cellularity is affected by aging in mdx mice.***

Representative HE staining of thymus from 3m and 9m C57Bl and mdx mice (n=4 each) (a). Immunofluorescence staining for the expression of Myod+ cells in cortex and medulla (b) and of CD11b+CD11c+ cells (c) from 3m and 9m C57Bl and mdx mice (n=4 each). Histograms showing the quantification of medulla/cortex ratio; of MyoD+ cells; of vascularized area (d) an CD11b+CD11c+ cells (e) in 3m and 9m C57Bl and mdx mice (n=4 each).

*Data information: data are presented as mean ± SD (**p<0.01; ****p<0.0001; Student t-Test with Welch's correction).*

To precisely determine the effects of these morphological changes in thymi cellularity, we performed FACS analysis: as we did not find differences in the amount of CD3+ T-cells (Fig. 6.1A), the percentage of single-positive (SP) CD4+ T-cells was significantly upregulated in 3m mdx mice related to age-matched C57Bl and 9m mdx (Fig. 6.1B): intriguingly, we found a down-regulation of CD4+ cells expressing both IFN-γ and IL17 related 9m mdx mice and 3m C57Bl (Fig. 6.1B). Similar to CD4+ cells, we found an up-regulation of SPCD8+ T-cells and the down-regulation of CD8+ cells expressing Cd69, IFN-γ and IL17 in 3m mdx compared to 9 mdx mice and 3m C57Bl (Fig. 6.1C). Myeloid CD11+ CD45+ cells were upregulated in 3m C57Bl related to 3m mdx and older C57Bl mice (Fig. 6.1D). Regarding the expression of double positive CD8+CD4+ T-cells, we evidenced a diminished percentage in 3m mdx tissues as well as for the CD8+CD4+IFN-γ+ and CD8+CD4+IL17+ T-cells while we demonstrated that aged 9m mdx mice over-expressed the CD8+CD4+CD69+ T-cells related to 3m mdx mice (Fig. 6.1E). Interestingly, we found that iNKT cells were upregulated in 3m C57Bl, while all the other subpopulations of iNKT were significantly over-expressed in 9m mdx related to 3m mdx mice and age-matched control animals (Fig. 6.1F). Similarly, the percentage of MAIT cells expressing IFN-γ and IL17 was increased in 9m mdx mice while these cells diminished in 3m mdx according to age-matched C57Bl mice (Fig. 6.1G). The paucity of unconventional T-cells in 3m mdx mice was confirmed also for γδ T-cells and their subpopulations expressing CD69 and IFN-γ: intriguingly, these cells were up-regulated in 9m mdx thymi (Fig. 6.1F).

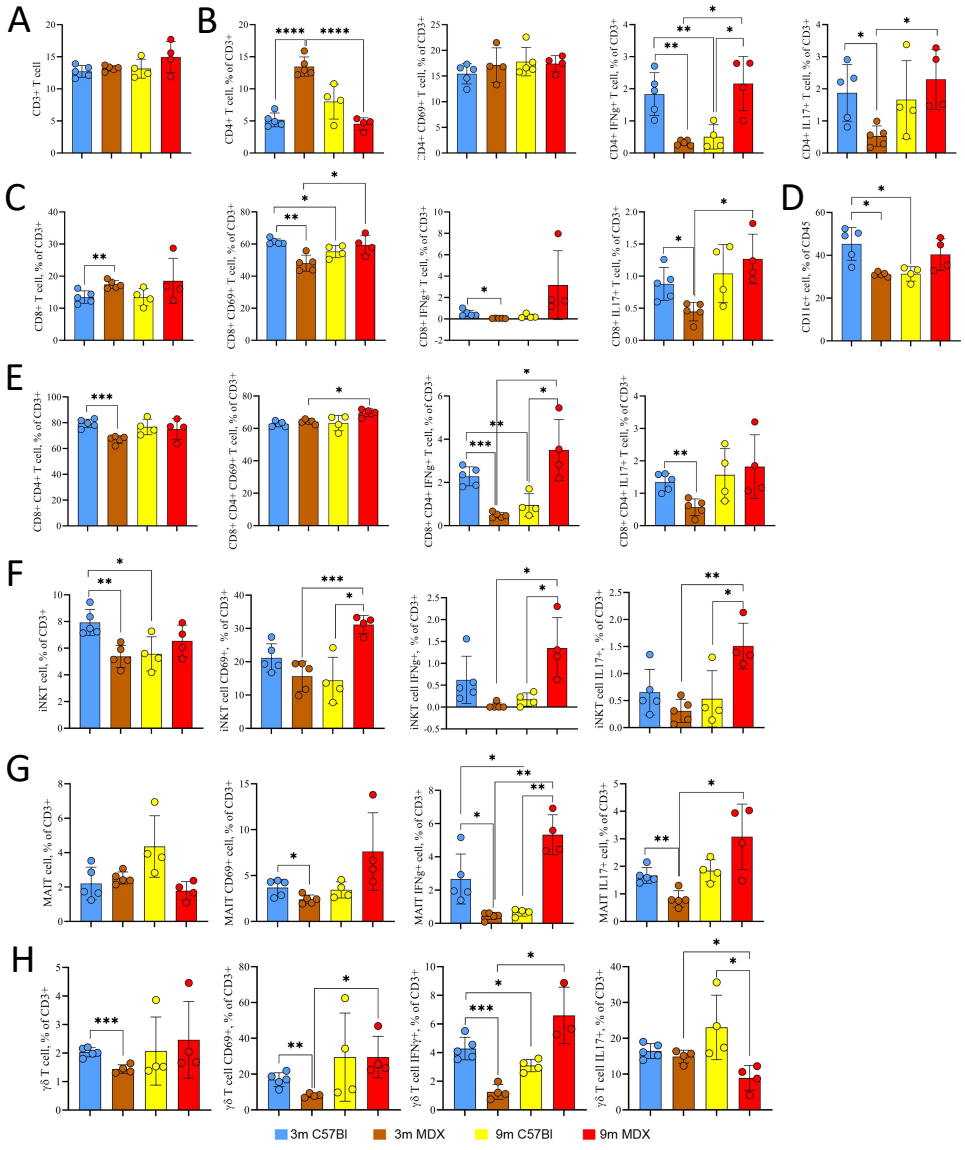

Figure 6.1. ***Thymic conventional and unconventional T-cells evaluation in 3m and 9m mdx mice.***

FACS analysis of immune cells from thymus of 3m C57Bl (n=5), 3m mdx (n=5), 9m C57Bl (n=4) and 9m mdx (n=4). Graphs show cumulative frequencies of conventional CD3+ T cells (a); single-positive CD4+ T-cells and subpopulations expressing CD69, IFN-γ and IL17 (b); single-positive CD8+ T-cells and subpopulations expressing CD69, IFN-γ and IL17 (c); CD45+CD11c+ myeloid cells (d); double-positive CD4+CD8+ T-cells and subpopulations expressing CD69, IFN-γ and IL17. Graphs show cumulative frequencies of unconventional CD3+ iNKT (f), MAIT (g) and γδ (h) T-cells expressing CD69+, IFN-γ+ and IL17+ markers.

*Data information: data are presented as mean ± SD (*p<0.05; **p<0.01; ***p<0.001; ****p<0.0001; Student t-Test with Welch's correction).*

DEPLETED GUT MICROBIOTA IN AGED mdx MICE AFFECTS IMMUNE RESPONSES AND MODULATES MUSCLE METABOLISM AND MORPHOLOGY

Microbial signals, such as microbial-associated molecular patterns (MAMPs) and metabolites, can be transported via the bloodstream and reach the thymus, where interact with thymic epithelial cells and influence the selection and education of developing T cells. Thus, perturbation of gut microbiota should represent a model for understanding the contribution of conventional T cell in muscle disease of mdx mice, as iNKT and MAIT cells are either absent or expressed at barely detectable levels in these animal models, as previously reported[87,88]. We initially investigated the impact of gut microbiota depletion on lymphocyte populations in 9m ABX-treated mdx mice. We observed that the percentage of splenic CD4+ T cells was lower in both 9m mdx mice and 9m mdx+ABX mice compared to age-matched C57Bl mice. However, no significant changes were found among the groups in CD8+ T cell populations (Fig. 7A). Similarly, in muscle tissue from 9m mdx mice, we observed a high abundance of CD4+ and CD8+ T cells, with no differences between the ABX-treated and untreated groups (Fig. 7B). Nevertheless, ABX treatment led to a reduction in splenic CD4+ IFN-γ-producing cells in 9m mdx mice, as confirmed by FACS analysis (Fig. 7C). Additionally, altered immune activation was observed in central memory and effector CD4+ T cell subsets in the spleen of ABX-treated mdx mice (Fig. 7D). To further support our findings, we examined whether disruption of the gut microbiota using antibiotics had effects on lymphocyte subsets in skeletal muscle of 9m mdx mice. We observed significant modulation of immune cell populations in the muscles of 9m mdx+ABX mice compared to 9m mdx mice, including an upregulation of central memory CD4+ cells, central memory CD8+ cells, and effector CD4+ cells (Fig. 7E).

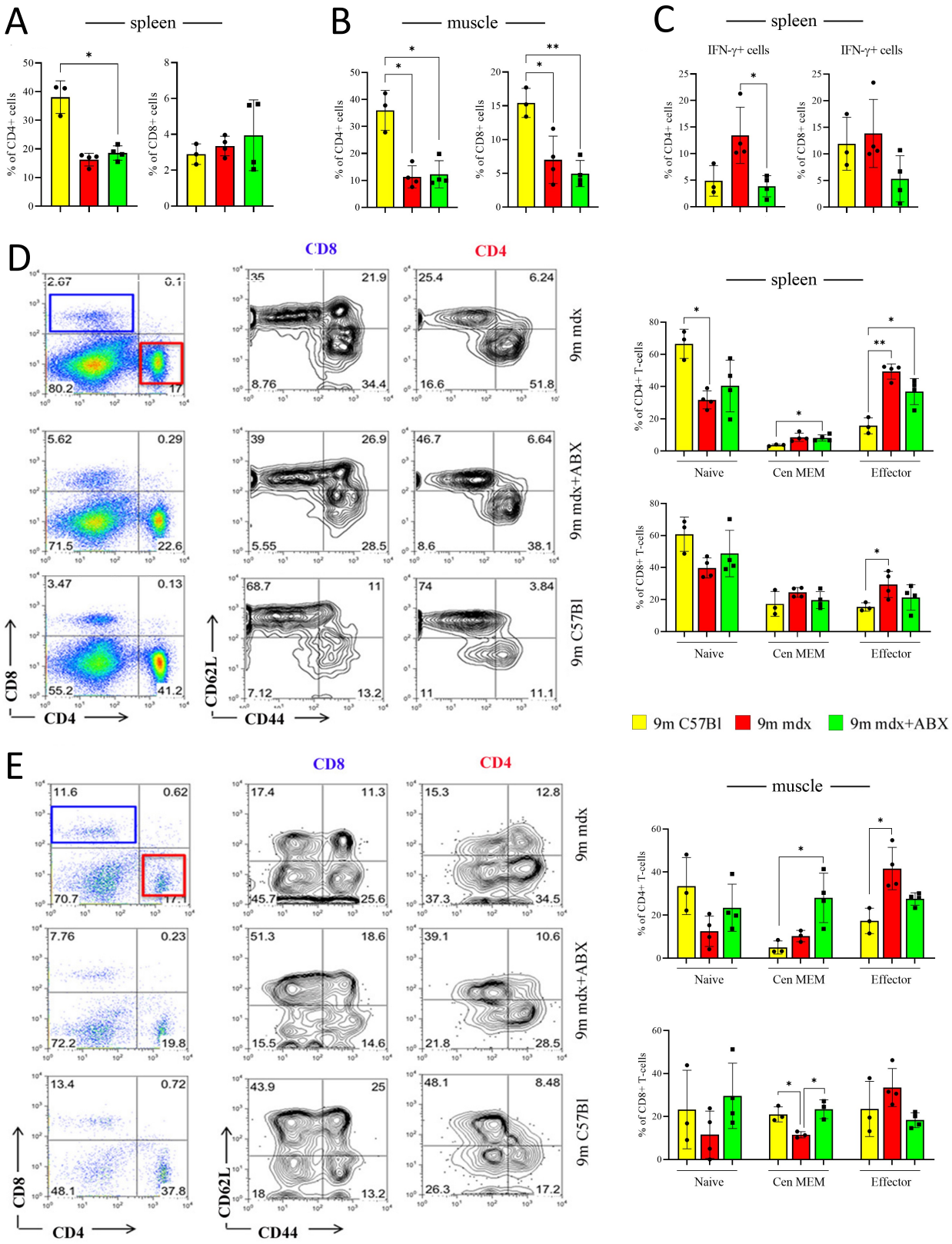

Figure 7. ***Spleen and muscle immune cells' modulation in 9m mdx+ABX mice***

FACS analysis of spleen and muscle homogenates from 9m C57Bl (n=3), 9m mdx (n=4) and 9m mdx+ABX (n=4). Graphs show cumulative frequencies of CD4 and CD8 T cells on live cells in the spleen (a) and muscle (b). (c) Graphs show

cumulative frequencies of IFN□□-producing splenic T cells. Representative dot-plots depicting CD4 and CD8 T cell subpopulations and relative cumulative frequencies in the spleen (d) and in the muscle (e). Gate strategy for cytometry quantification of spleen (d) and muscle (e) CD4+ and CD8+ T cell naïve, central memory and effector compartments are shown.

*Data information: data are presented as mean ± SD (*p<0.05; **p<0.01; One Way ANOVA Kruskal-Wallis test).*

In 9m germ-free mdx (GFmdx) mice, we observed a slight downregulation of splenic innate cells, including granulocytes, macrophages, and monocytes (Fig. 8A). Furthermore, we demonstrated a significant decrease in the abundance of CD4+ cells in the spleen of GFmdx mice compared to age-matched mdx and C57Bl mice (Fig. 8B). However, regulatory T cells (Tregs) were not affected by the germ-free condition (Fig. 8C). Regarding the subpopulation of CD4+/CD8+ cells, we found a significant upregulation of CD4+ and CD8+ naive cells and a downregulation of effector memory cells in GFmdx mice compared to 9m mdx and C57Bl mice (Fig. 8D, E). In skeletal muscle cells, we observed a drastic reduction in CD45+ infiltrating cells in 9m GFmdx mice compared to age-matched mice (Fig. 8F). Furthermore, muscle-derived CD4+ cells were diminished in 9-month-old GFmdx mice compared to age-matched C57Bl mice, while CD8+ cells and Tregs did not show significant variations (Fig. 8G, H). Interestingly, CD4+ effector memory cells were upregulated in 9-month-old GFmdx mice compared to C57Bl mice (Fig. 8I, J). Without any doubts, we observed an ablation of T naive cells in both GFmdx and antibiotic-treated (ABX) mice. However, there was an increase in naive CD4+ T cells due to a reduced response to endogenous antigens. Despite the abrogation of thymic export under ABX or GF conditions, immune homeostasis in the periphery did not appear to be compromised. This may be attributed to the deactivation of CD4/CD8 T cells, which could explain the reduction in immune pathology in chronic inflammation of mdx. These findings suggest the existence of a compensatory homeostatic mechanism in response to the loss of thymic output.

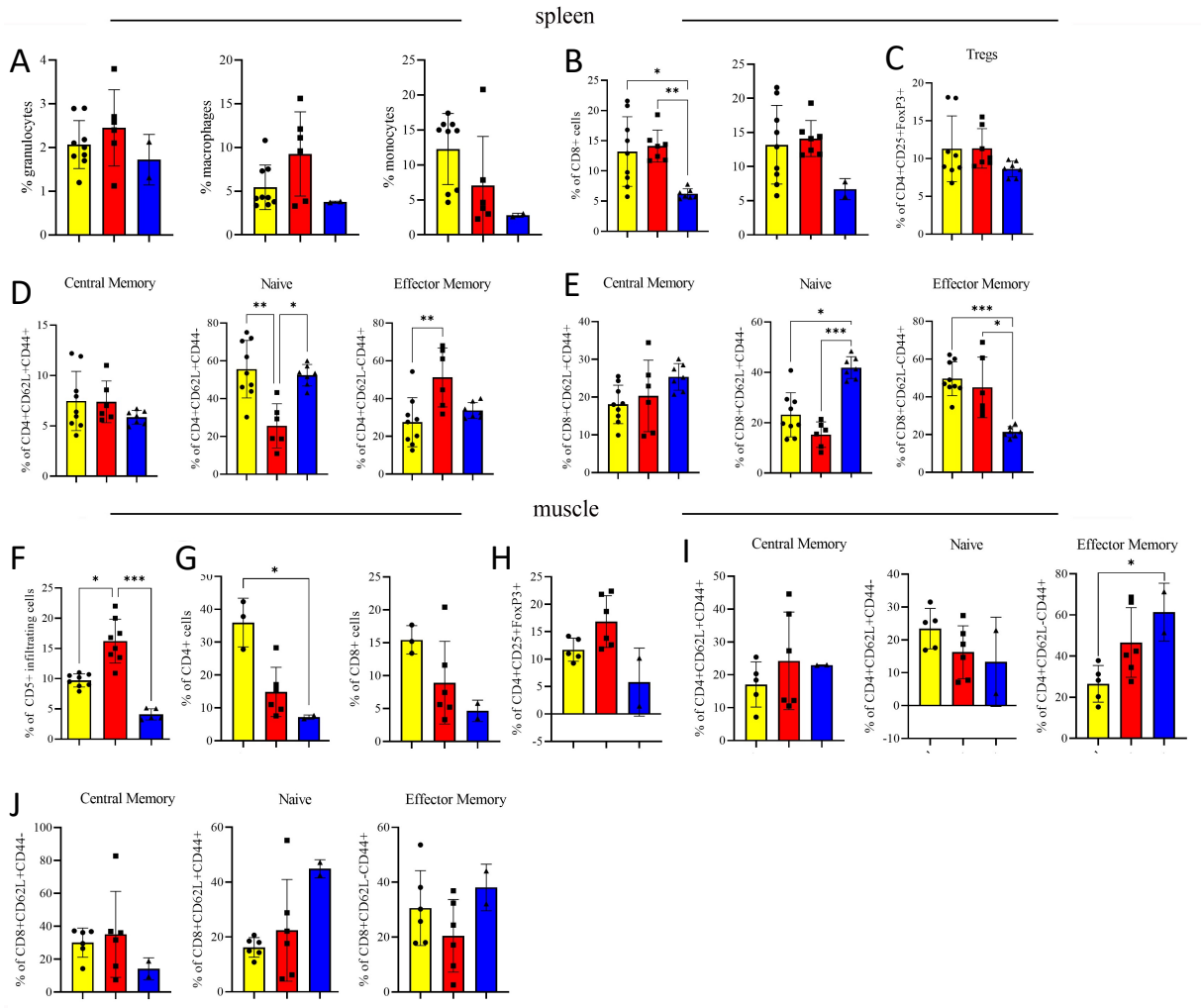

Figure 8. ***Spleen and muscle immune cells' modulation in 9m GFmdx mice***

FACS analysis of spleen and muscle homogenates from 9m C57Bl (n=8), 9m mdx (n=6) and 9m GFmdx (n=7). Graphs show cumulative frequencies of splenic (a) innate immune cells – granulocytes, macrophages, monocytes; (b) adaptive immune CD4+/CD8+ cells and (c) Tregs. Frequency evaluation of (d) CD4+ and (e) CD8+ subpopulations, as central memory, naïve and effector memory cells. Graphs show cumulative frequencies of muscular (f) CD45+ infiltrating cells, (g) CD4+/CD8+ cells and (h) Tregs. Frequency evaluation of (i) CD4+ and (j) CD8+ subpopulations, as central memory, naïve and effector memory cells.

*Data information: data are presented as mean ± SD (*p<0.05; **p<0.01; One Way ANOVA Kruskal-Wallis test).*

Regarding the architecture of skeletal muscle, the fiber-type distribution was not affected by ABX in older mdx but changed significantly in 9m GFmdx, as their distribution showed a significant upregulation of smaller fibers (Fig. 9A). According to the observed emerging role of the gut microbiota on skeletal muscle physiology, the cross-sectional areas (CSAs) of the myofibers observed in the muscles of 9m mdx+ABX and GFmdx mice were significantly lower than those

observed in the muscles of 9m mdx (mean area for TA ± SEM: 9m C57Bl: 1911 ± 6.7 μm2 N=20682; 9m mdx, 2292 ± 16.17 μm2 N=15855; 9m+ABX mdx 1636.55 ± 8.31 μm2 N=25061; 9m GFmdx 1172.10 ± 7.12 μm2 N=19524). In line, the values of frequency distribution confirmed the smaller area of myofibers in mice with depletion of microbiota, in particular 9m GFmdx mice (25% Percentile: 9m C57Bl: 1175.384; 9m mdx+ABX: 678.447; 9m mdx: 848; 9m GFmdx: 524.69. 75% Percentile: 9m C57Bl: 2529.613; 9m mdx+ABX: 678.447; 9m mdx: 3035; 9m GFmdx: 1486.209) (Fig. 9A). Concomitantly, there was also a decrease of muscle fibrosis in the ABX-treated and GFmdx mice (mean % area of TA fibrosis for 9m C57Bl: 2.46; 9m mdx+ABX: 16.07; 9m mdx: 18.72; 9m GFmdx: 9.97; each difference $p<0.0001$ except for 9m mdx vs 9m mdx+ABX) (Fig. 9B). The amount of myosin isoforms did not show significant changes in dystrophic mice following ABX treatment or in GFmdx mice. However, significant differences were observed for the IIa and IIb isoforms compared to 9-month-old C57Bl mice. Notably, we found significant differences in the expression of myosin I between 9-month-old mdx+ABX mice and 9-month-old GFmdx mice (Fig. 9C). Staining for succinate dehydrogenase (SDH) in GFmdx muscles demonstrated the upregulation of SDH+ myofibers compared to untreated and control mice (Fig. 9D). As expected, the expression of serum markers of inflammation such as alanine aminotransferase (ALT) and aspartate aminotransferase (AST) were upregulated in mdx mice compared to control mice. However, we observed a slight decrease in their values following microbiota depletion (Fig. 9E). Similarly, creatine phosphokinase (CPK) levels were mainly upregulated in dystrophic mice, while GFmdx mice showed a slight but significant overexpression compared to 9-month-old C57Bl mice (Fig. 9E).

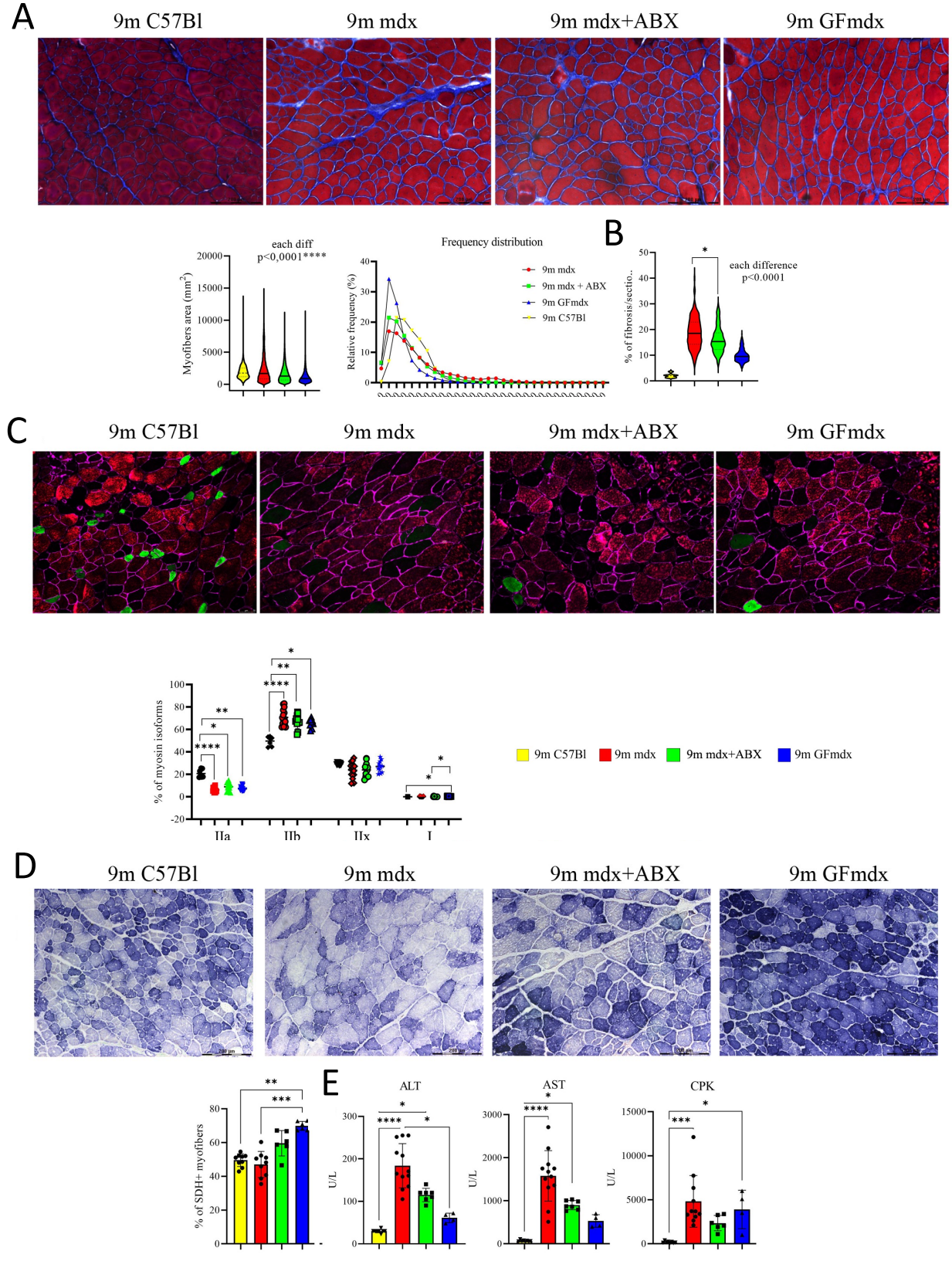

Figure 9. ***Skeletal muscle morphology modulation in mdx mice lacking microbiota***

(a) Representative Trichrome-Gomori staining and quantification of myofiber area and relative frequency of the myofiber cross-sectional area (CSA) expressed as the frequency distribution of the TA muscles of 9m C57Bl (n=), 9m

mdx (n=), 9 mdx+ABX (n=) and 9m GFmdx (n=) mice. For morphometric analysis, images were quantified with Image J software for each mouse. Scale bars: 2000 μm. (b) Graph showing the percentage of fibrosis in TA of the mice in all the groups. (c) Representative images of skeletal muscle showed the distribution and composition of the myosin heavy chain (MyHC) isoforms (Type IIa, IIx and IIb; Type I). Graph portrays the percentage of myofibers expressing significantly different MyHC isoforms in TAs of 9m C57Bl (n=), 9m mdx (n=), 9 mdx+ABX (n=) and 9m GFmdx (n=) mice (n= images per animal). Scale bars: 50 μm. (d) Representative staining and quantification of SDH+ myofibers percentage of TAs from 9m C57Bl (n=), 9m mdx (n=), 9 mdx+ABX (n=) and 9m GFmdx (n=) mice (n= images per slide). Scale bars: 200 μm. (e) ALT, AST and CPK quantification in the serum of 9m C57Bl (n=), 9m mdx (n=), 9 mdx+ABX (n=) and 9m GFmdx (n=) mice.

*Data information: data are presented as mean ± SD (*p<0.05; **p<0.01, ***p<0.001, ****p<0.0001; One-Way ANOVA Kruskal-Wallis test).*

Since the aging process that naturally occurs in muscle determine the atrophy or sarcopenia, we followed the expression of FOXO1 and – also – of the FOXO dependent autophagy-related proteins[89]. FOXO1 was detected only in 9m mdx and 9m mdx+ABX mice, no changes were reported in in autophagosome related LC3 while the modulation of ATG-7 and P62 may be ascribable to an autophagic flux disruption (Fig. 10A). The over-expression of SDH+ fibers in microbiota-depleted mice prompted us to monitor the mitochondrial activity in skeletal muscle. The mitochondrial TOMM20 content was down-regulated in 9m mdx+ABX and 9m GFmdx as well as DRP-1 and COX-4, suggesting dysfunctions affecting mitochondria in these animals (Fig. 10B). This condition was hampered by differences in PPAR-γ, whose function in mitochondrial biogenesis is well described[90], and PKC-θ, that is associated with mitochondrial-dependent apoptosis[91] and ROS production[92] (Fig. 10B). Next, we focused on HDACs, that are commonly over-expressed in mdx mice[93] and actively participate into regulation of metabolism and inflammation[94,95]. The immunoblot analysis of skeletal muscles showed that HDAC1 and HDAC2 were expressed mainly in 9m mdx and 9m mdx+ABX (Fig. 10C). Indeed, we assessed the expression of NF-kB and Proto-Oncogene-NF-kB Subunit (RelB) that resembled that of HDACs (Fig. 10C). As expected we found the up-regulation of atrophic markers – namely atrogin and MuRF-1 – in GFmdx and mdx+ABX mice (Fig. 10D) while we did not find the expression of mTOR but, surprisingly, we noted that the mTOR effectors 4EBP1 and S6RB were significantly modulated in muscular tissues (Fig. 10E).

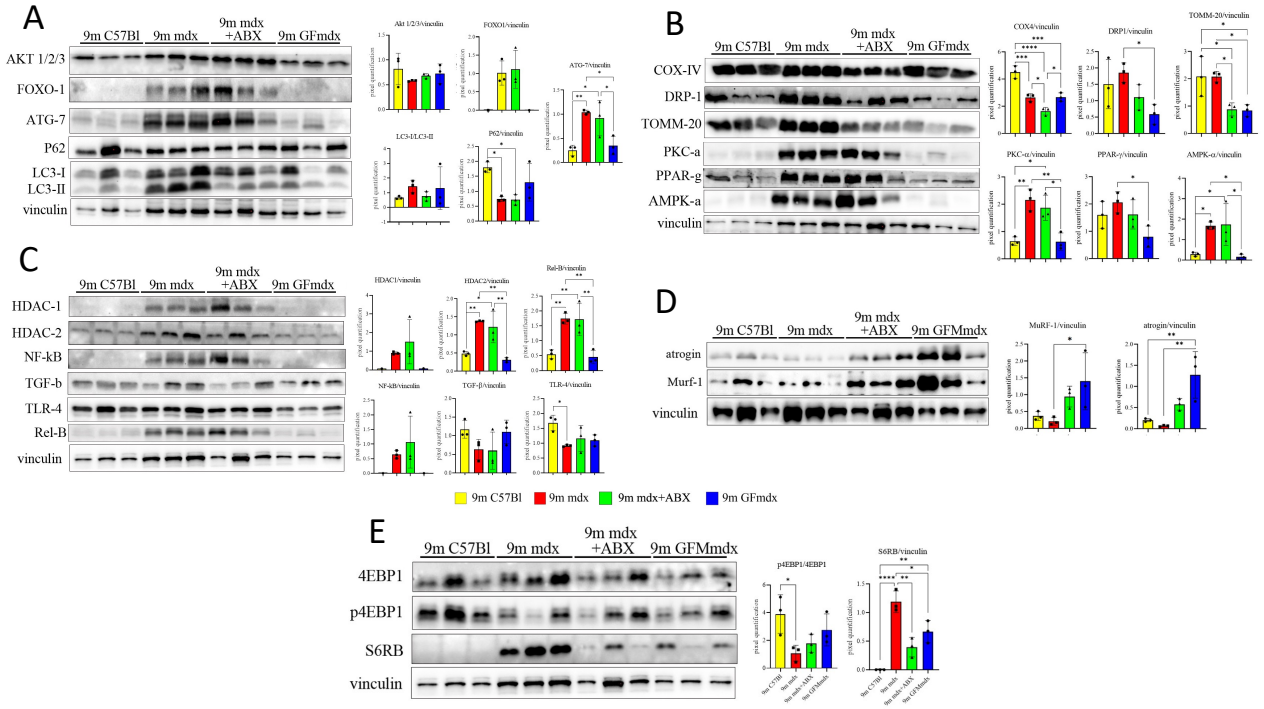

Figure 10. ***Proteomic evaluation of pathological phenotype in in mdx mice lacking microbiota***

Cropped images of representative WB analysis of TA muscle of 9m C57Bl, 9m mdx, 9 mdx+ABX and 9m GFmdx mice (n=3 each) mice showing the expression of the proteins specifically involved in (a) atrophy and apoptosis; (b) mitochondrial biogenesis and function; (c) inflammation; (d,e) atrophic markers.

RNA-SEQ ANALYSIS REVEALED CONVERGENT PATHWAYS IN 3M AND 9M mdx MUSCLE DEPENDING ON MICROBIOTA

We thus performed RNA-seq on muscles of 9m mdx+ABX and 9m GFmdx compared to age-matched mdx. PCA analysis of RNA-seq datasets demonstrated treatment-dependent clustering of samples, differentiating ABX and GF mdx from mdx controls (Fig. 11A). To detect the gene expression trends that were induced by treatments in mdx muscle throughout the age, we overlayed the convergent gene trends at 3 and 9 months of age (Suppl. Fig. 3A, B). We found 6585 genes whose expression trend was convergent according to treatment and age (Fig. 11B). Of those, 1481 genes were upregulated by both ABX and GFmdx over time, while 5105 were downregulated. GO analysis of the age-convergent upregulated genes showed a clear enrichment for catabolic and autophagic processes, often associated with muscle atrophy and wasting. Conversely, GO analysis of the age-convergent downregulated genes still confirmed the downregulating effects of both ABX and GF mdx on inflammation and fibrosis gene pathways (Fig. 11B). ABX and GF mdx convergently upregulated markers of autophagy and negative mass remodeling in mdx muscle at both 3 and 9

months of age (Trim63, Atf4, Gaff45a, Map1lc3a/b, Bnip3, Smad3). Interestingly, Tripartite Motif Containing 63 (Trim63/MuRF1) coordinates the autophagy pathway that modulates the basal and atrophy-induced turnover of the muscular form of CHRN (cholinergic receptor, nicotinic/nicotinic acetylcholine receptor)[96]. Activating Transcription Factor 4 (Atf4) is activated by stress response and it is fundamental to correlate autophagy with unfolded protein response[97] while Growth Arrest DNA Damage Inducible Alpha (Gaff45a) is a key gene to link autophagy and muscle metabolism[98]. Myogenic markers like Myog and Pax7 were also convergently downregulated over time (Fig. 11C). In addition, gene markers of inflammation and fibrosis (Nfkb2, Postn, Tnf, Ltbp4) were found convergently downregulated over time, suggesting a long-term effect of microbial ablation on fibroinflammatory remodeling of mdx muscle (Fig. 11D). Many genes associated with fibrosis and extracellular matrix remodeling (Adamts, Col, Lamb, Mmp gene families, as well as Fn1 and Itga8) were downregulated by both ABX and GF in mdx muscle at 3 and 9 months of age (Fig. 11D). Fibronectin 1 (Fn1) is dramatically diminished in aged stem cell niche of skeletal muscle leading to inhibition of satellite cells proliferation[99] and – together with other Mmp genes – was suggested as anti-fibrogenic target[100]. Integrin alpha-8 (Itga8) is determinant in the development of lung fibrosis[101] and it is often associated to Col13a1 gene in fibroblasts[102].

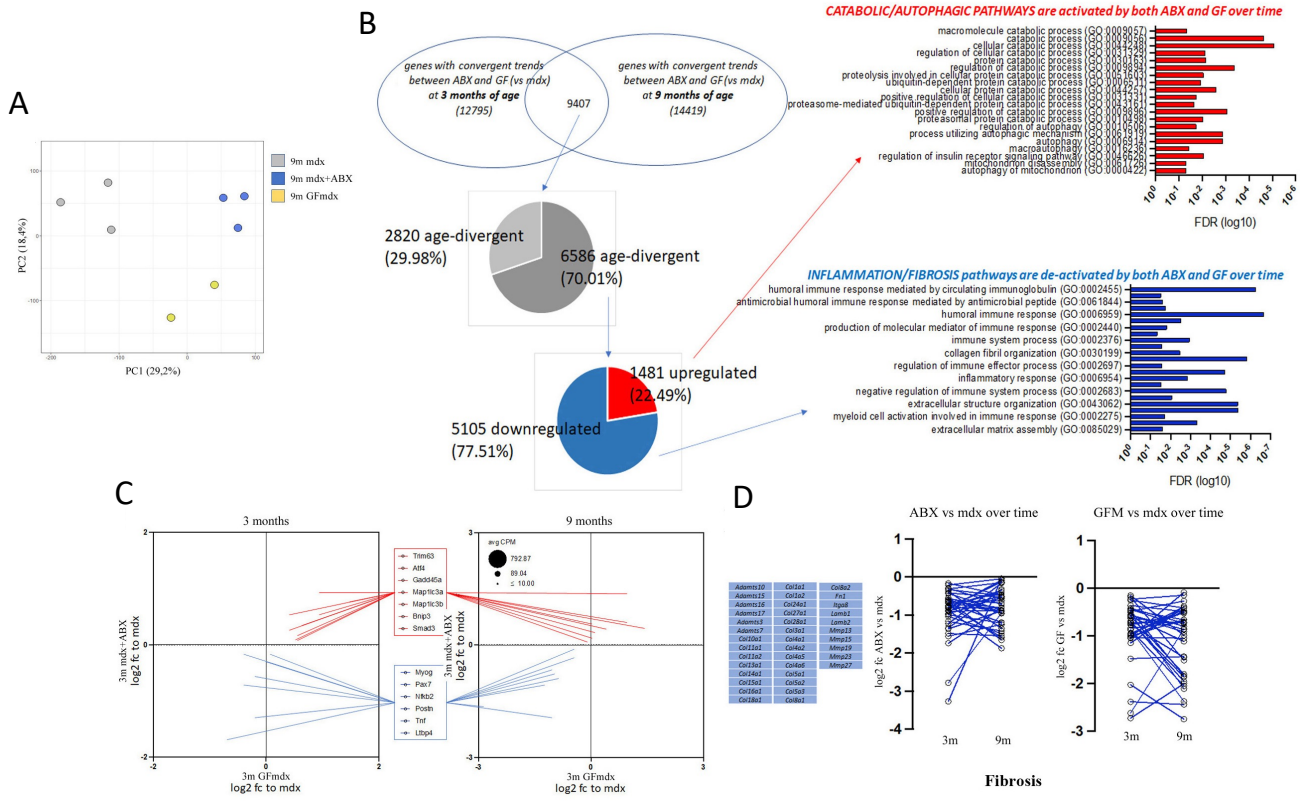

Figure 11. ***Go analysis of RNAseq datasets of skeletal muscles of old ABX-treated and GFmdx mice***

(a) PCA analysis of RNA-seq datasets of TA muscle of 9m mdx, 9m mdx+ABX and 9m GFmdx. (b) GO analysis of the age-convergent/divergent up and downregulated genes. (c) Myogenic, inflammatory, and fibrotic gene markers convergently downregulated by both ABX and GF conditions in young and older mdx mice.

DISCUSSION and CONCLUSIONS

The age-related deterioration of tissue structure and physiological function is frequently accompanied by detrimental modulation of the immune system. In the context of aging, the innate immune system experiences a decline in proliferation and activity of neutrophils, dendritic cells, and natural killer cells. Additionally, macrophages upregulate the expression of pro-inflammatory cytokines, such as IL-6 and IL-8. Concurrently, significant changes occur in the adaptive immune system following thymus atrophy. Naive and Th1 T-cells decrease, while memory T and Th2 T-cells increase. Importantly, the inhibition of B cell antibody production negatively affects helper T-cell activation[103]. In DMD, muscular degeneration is driven by inflammation and cell invasion triggered by DAMPs released by injured myofibers, oxidative stress, and impaired calcium handling. Asynchronous cycles of muscle fiber regeneration and degeneration exacerbate the muscle infiltration of immune cells, along with their secretion of pro-inflammatory cytokines. The severity of muscle injury and inflammation determines changes in muscle structure, such as modifications in fiber type and increased connective and fat content[104,105], which worsen with age, contributing to DMD muscle weakness[106]. Considering the various factors influencing the aging phenotype in the context of DMD, multiple pathological sources have been investigated. As mentioned in the introduction section, metabolites, and microbial products, including PAMPs, may contribute to muscle atrophy and immune system activation in DMD patients due to altered intestinal permeability [107,108]. In this study we provide insights into the impact of aging and muscular dystrophy on the gut microbiota composition. The observed differences between healthy and dystrophic mice, as well as the age-related changes in microbiota composition, could have implications for understanding of how the gut microbiota interacts with these conditions and may offer potential avenues for further research and therapeutic interventions. We chose to analyze both 3m mdx, given that inflammation and muscle damage occur at this age and 9m mdx, to evaluate the role of aging in the development of the pathology and to consider the cardiac involvement[109].

We found that mdx mice, irrespective of age, showed reduced enrichment of amplicon sequence variants (ASV) compared to age-matched wild-type C57Bl mice. This indicates the presence of dysbiosis in the gut microbiota of mdx mice, which is in line with our previous research[108]. Dysbiosis often implies an imbalance in the composition of the gut microbiota and can have various health

implications. It was observed that the differences in microbiota composition between younger and older mice were less pronounced in both mdx and C57Bl mice. This suggests that aging itself can lead to changes in the gut microbiota composition, which is an interesting finding and may have implications for age-related health issues. Moreover, principal Coordinates Analysis (PCoA) revealed a distinct separation between healthy and dystrophic mice, indicating that the microbiota of these two groups is significantly different. Among specific microbial abundance changes, the Helicobacter, Firmicutes, and Clostridium were found to be abundant in 9-month-old C57Bl mice, while Bacteroides, Prevotella, and Odoribacter were upregulated in age-matched mdx mice. Interestingly, Prevotella, Alistipes, Anaeroplasma, and Odoribacter were identified as common signatures in mice with DMD. This indicates that these microbes might play a significant role in the context of DMD and could be potential targets for further research or therapeutic interventions. When comparing 3-month-old and 9-month-old mice, the study observed changes in microbial composition in both C57Bl and mdx mice. For example, Akkermansia and Lactobacillus were upregulated in younger C57Bl mice, while Helicobacter and Alistipes were more abundant in 3-month-old mdx mice. These findings demonstrate that age-related changes in gut microbiota composition are not limited to dystrophic mice but are also present in healthy mice. We thus reconstructed metabolic pathways using metabolites with high discriminatory power. The most enriched sets of metabolites in dystrophic mice were associated with antibiotics biosynthesis, galactose metabolism, sucrose metabolism, and lipid metabolism. Dystrophic mice showed upregulation of 3-phenyllactic acid; however, the metabolome of 9-month-old C57Bl mice was distinct from that of all other animals. These pathway enrichments suggest potential metabolic alterations in response to aging and dystrophy.

We further investigated the potential impact of changes in the gut microbiota and the presence of specific metabolites, such as riboflavin and short-chain fatty acids (SCFAs), on immune cell populations focusing on conventional and unconventional T cells. Riboflavin metabolism was found to be upregulated in 9-month-old mdx mice. The study suggests that SCFAs could influence the antimicrobial activity of mucosal-associated invariant T cells (MAIT) and the pro-inflammatory switch of invariant natural killer T cells (iNKT), potentially affecting these cell populations. In the spleen of 9-month-old C57Bl mice, there was an upregulation of CD3+ cells, while their abundance diminished with aging in mdx mice. CD8+ T-cells were notably upregulated in 9-month-old C57Bl mice, while CD8+ inflammatory subpopulations expressing CD69+, IFN-γ, and IL-17 were upregulated in dystrophic mice but slightly diminished with age. Interestingly, iNKT cells and

activated MAIT cells were significantly increased in the spleen of older mdx mice compared to age-matched C57Bl mice. These data suggest a correlation between riboflavin levels and the activation of spleen-derived MAIT and iNKT cells. Colonic CD3+ T-cells were upregulated in 3-month-old mdx mice compared to age-matched C57Bl and 9-month-old mdx mice. CD8+ T-cells were also over-expressed in 3-month-old mdx mice and 9-month-old C57Bl mice. Furthermore, the number of iNKT and MAIT cells in the colon of older C57Bl and mdx mice decreased compared to younger ones, potentially related to reduced levels of SCFAs in the colon. In hindlimb muscles, 3-month-old mdx mice showed an increase in CD4+ T-cells, while dystrophic mice up-regulated CD8+ cells. CD45+CD11+ myeloid cells were more abundant in 3-month and 9-month mdx mice, and γδ T-cells expressing CD69+ were over-expressed in dystrophic mice. These findings collectively suggest complex interactions between gut microbiota, metabolites, and immune cell populations in different tissues highlighting the potential role of gut-derived metabolites on unconventional T cells in age-related changes of muscular dystrophy. To better understand the role of T cells in the context of muscular dystrophy, we characterized their development in the thymus tissue considering also that thymic involution is an age-related decline in thymus size and function. In the context of dystrophic mice, we noted that in 3-month-old mdx mice, there was a down-regulation of the medullary/cortex ratio compared to age-matched C57Bl mice. Conversely, in older mdx mice (9 months), there was an upregulation of this ratio compared to both age-matched C57Bl and younger mdx mice. Medullary/cortex ratio showed a down-regulation with age in C57Bl mice, and conversely an upregulation in mdx mice. These changes in thymic architecture may have significant and long-term effects on T-cell development. Thymic myoid cells, which share structural similarities with muscle cells, were evaluated for their presence in the thymus. These cells have been associated with enhancing autoimmune responses. The study found that MyoD+ cells were more abundant in 3-month-old C57Bl mice compared to 9-month C57Bl and 3-month mdx mice. Interestingly, MyoD+ cells in 9-month mdx mice were comparable to those in younger mice suggesting a potential role of MyoD+ cells in central tolerance in dystrophic conditions. Since dendritic cells (DCs) in the thymus play a relevant role in central tolerance formation, we investigated DCs thymic populations in both young/older wild type and dystrophic mice. We found that aging caused a down-regulation of CD11c+CD11b+ DCs in C57Bl mice but led to an over-expression in mdx mice. Furthermore, age-related changes were observed in the number of DCs in both C57Bl and mdx mice. These findings suggest modulatory effects on autoreactive thymocyte screening, which could influence immune tolerance. FACS analysis was performed to evaluate

thymic cellularity. While there were no differences in the amount of CD3+ T-cells, there were significant changes in the percentages of single-positive (SP) CD4+ and CD8+ T-cells, which are indicative of T-cell development. For example, 3-month mdx mice exhibited an upregulation of SP CD4+ T-cells compared to age-matched C57Bl and 9-month mdx mice. Various subpopulations of T-cells, including those expressing CD69, IFN-γ, and IL17, showed age-related changes and differences between mdx and C57Bl mice. Moreover, iNKT cells were upregulated in 3-month C57Bl mice, while in 9-month mdx mice, the iNKT cells were significantly over-expressed compared to both 3-month mdx mice and age-matched control mice. Interestingly, MAIT cells expressing IFN-γ and IL17 were increased in 9-month mdx mice but diminished in 3-month mdx mice relative to age-matched C57Bl mice. Similar age-related changes and differences between mdx and C57Bl mice were observed in γδ T-cells and their subpopulations expressing CD69 and IFN- γ. Overall, these data confirmed age- and disease-related changes in T-cell development and unconventional T cell subpopulations that could have implications for immune tolerance in muscular dystrophy.

To sustain these evidences, we examined the impact of gut microbiota manipulation on immune cell populations and muscle characteristics in mdx mice. Depletion of gut microbiota through antibiotic treatment (ABX) in 9-month-old mdx mice resulted in a reduction of splenic CD4+ T cells but no significant changes in CD8+ T cell populations. Muscle tissue from 9-month-old mdx mice exhibited high abundance of both CD4+ and CD8+ T cells, and ABX treatment did not significantly alter these populations. In ABX-treated 9-month-old mdx mice, there was a reduction in splenic CD4+ IFN-γ-producing cells. Moreover, immune activation patterns were altered in central memory and effector CD4+ T cell subsets in the spleen of ABX-treated mdx mice. Gut microbiota depletion caused significant modulation of immune cell populations in the muscles of 9-month-old mdx mice, including an upregulation of central memory CD4+ and CD8+ cells and effector CD4+ cells.

Interestingly, 9-month-old germ-free (GF) mdx mice, showed a reduction in splenic innate cells and CD4+ cells compared to age-matched mdx and C57Bl mice. Although the regulatory T cells (Tregs) were not significantly affected by the germ-free condition, the subpopulations of CD4+/CD8+ cells showed changes, with an upregulation of naive CD4+ and CD8+ cells and a downregulation of effector memory cells in GFmdx mice compared to age-matched mdx and C57Bl mice. Importantly, total CD45+ and T CD4+ infiltrating cells in skeletal muscle were drastically reduced despite CD4+ effector memory cells were upregulated in 9-month-old GFmdx mice compared to C57Bl mice.

The fiber-type distribution was not significantly affected by ABX treatment in older mdx mice but changed significantly in 9-month-old GFmdx mice, with an upregulation of smaller type I and SDH+ fibers. In line, cross-sectional areas of myofibers were significantly lower in the muscles of 9-month-old mdx+ABX and GFmdx mice compared to untreated 9-month-old mdx mice. Additionally, muscle fibrosis was decreased in both ABX-treated and GFmdx mice. RNA-seq analysis revealed that treatment with ABX and GF caused treatment-dependent clustering of samples, differentiating these groups from mdx controls. Convergent gene expression trends were observed in 6585 genes that were both upregulated and downregulated by ABX and GF over time. GO analysis of the upregulated genes revealed enrichment for catabolic and autophagic processes, while downregulated genes were associated with inflammation and fibrosis pathways. The upregulated genes included those associated with autophagy and negative mass remodeling in mdx muscle, while the downregulated genes included those associated with inflammation and fibrosis. Gene markers related to fibrosis and extracellular matrix remodeling were downregulated in both ABX and GF mdx muscle. Notably, these analysis indicated that microbial manipulation had long-term effects on inflammation, fibroinflammatory remodeling, and muscle physiology.

The experiments of this work were designed to provide a global picture of the mucosal, immunological and microbial alterations concurring in determining the intestinal inflammatory environment in dystrophic mice. Taking into account the involvement of the immune system in mediating the pathophysiology of DMD, we aim to unveil the clinical significance of the balancing between innate and adaptive immunity, dissecting precisely the involvement of thymus in regulating different aspects of pathogenesis. In particular, with more specific analysis, we will deeply investigate those subsets of deregulated T cells – MAIT cells, Tregs, DCs – that directly or through the release of specific cytokines or the activation of specific receptor promote muscular damage. Thanks to transcriptomic analysis of these cells, we will widely analyze how immunity primary affects DMD opening new therapeutic scenario for these diseases. A limited number of studies focused on the impact of gut microbiota on muscle physiology. This way, in parallel, we plan to decipher how T-cells interact with microbiota in regulating the entero-thymic communications and consequently the spreading of inflammation in dystrophic background. This PhD thesis suggests that the gut microbiota has a significant influence on immune cell populations, muscle characteristics, and gene expression in mdx mice, potentially impacting muscle disease and inflammatory responses. Depletion of gut microbiota can lead to changes in immune cell

populations and muscle morphology, as well as alterations in the expression of genes associated with inflammation, fibrosis, and autophagy. These findings emphasized the complex relationship between the gut microbiota, the immune system, and muscle health in the context of muscular dystrophy. The approach used in this study will enable the identification of the fundamental molecular pathways underlying this entero-thymic-muscle axis and provide valuable insights into how the intestinal microbiota shape the inflammatory response and confer distinct susceptibility to muscle pathology. The aim of our study is to identify novel biomarkers associated with gastrointestinal involvement. Our aims are to predict disease progression and translate these findings into clinical practice, enabling patients to be stratified according to the most effective treatments. Additionally, our results will support the development of innovative therapeutic strategies to improve care for this debilitating disease.

REFERENCES

1 Ahmad, K., Shaikh, S., Ahmad, S. S., Lee, E. J. & Choi, I. Cross-Talk Between Extracellular Matrix and Skeletal Muscle: Implications for Myopathies. *Frontiers in pharmacology* **11**, 142, doi:10.3389/fphar.2020.00142 (2020).

2 Carberry, S., Zweyer, M., Swandulla, D. & Ohlendieck, K. Proteomics reveals drastic increase of extracellular matrix proteins collagen and dermatopontin in the aged mdx diaphragm model of Duchenne muscular dystrophy. *International journal of molecular medicine* **30**, 229-234, doi:10.3892/ijmm.2012.1006 (2012).

3 Emery, A. E. The muscular dystrophies. *Lancet* **359**, 687-695, doi:10.1016/S0140-6736(02)07815-7 (2002).

4 Cui, Q. *et al.* GXYLT2 accelerates cell growth and migration by regulating the Notch pathway in human cancer cells. *Experimental cell research* **376**, 1-10, doi:10.1016/j.yexcr.2019.01.023 (2019).

5 Demirdizen, E. *et al.* TRIM67 drives tumorigenesis in oligodendrogliomas through Rho GTPase-dependent membrane blebbing. *Neuro-oncology* **25**, 1031-1043, doi:10.1093/neuonc/noac233 (2023).

6 Haslett, J. N. *et al.* Gene expression comparison of biopsies from Duchenne muscular dystrophy (DMD) and normal skeletal muscle. *Proceedings of the National Academy of Sciences of the United States of America* **99**, 15000-15005, doi:10.1073/pnas.192571199 (2002).

7 Havugimana, P. C. *et al.* Scalable multiplex co-fractionation/mass spectrometry platform for accelerated protein interactome discovery. *Nature communications* **13**, 4043, doi:10.1038/s41467-022-31809-z (2022).

8 Huttlin, E. L. *et al.* Dual proteome-scale networks reveal cell-specific remodeling of the human interactome. *Cell* **184**, 3022-3040 e3028, doi:10.1016/j.cell.2021.04.011 (2021).

9 Kim, T. *et al.* Identification of LRRc17 as a negative regulator of receptor activator of NF-kappaB ligand (RANKL)-induced osteoclast differentiation. *The Journal of biological chemistry* **284**, 15308-15316, doi:10.1074/jbc.M807722200 (2009).

10 Muntoni, F., Torelli, S. & Ferlini, A. Dystrophin and mutations: one gene, several proteins, multiple phenotypes. *Lancet Neurol* **2**, 731-740, doi:10.1016/s1474-4422(03)00585-4 (2003).

11 Liu, F. *et al.* LRRc17 controls BMSC senescence via mitophagy and inhibits the therapeutic effect of BMSCs on ovariectomy-induced bone loss. *Redox biology* **43**, 101963, doi:10.1016/j.redox.2021.101963 (2021).

12 Martone, J. *et al.* SMaRT lncRNA controls translation of a G-quadruplex-containing mRNA antagonizing the DHX36 helicase. *EMBO reports* **21**, e49942, doi:10.15252/embr.201949942 (2020).

13 Mavillard, F. *et al.* Ablation of the carboxy-terminal end of MAMDC2 causes a distinct muscular dystrophy. *Brain : a journal of neurology*, doi:10.1093/brain/awad256 (2023).

14 Nagase, H., Yao, S. & Ikeda, S. Acute and chronic effects of exercise on mRNA expression in the skeletal muscle of two mouse models of peripheral artery disease. *PLoS One* **12**, e0182456, doi:10.1371/journal.pone.0182456 (2017).

15 Poveda, J. *et al.* MXRA5 is a TGF-beta1-regulated human protein with anti-inflammatory and anti-fibrotic properties. *Journal of cellular and molecular medicine* **21**, 154-164, doi:10.1111/jcmm.12953 (2017).

16 Shen, Y. *et al.* Matrix remodeling associated 7 proteins promote cutaneous wound healing through vimentin in coordinating fibroblast functions. *Inflammation and regeneration* **43**, 5, doi:10.1186/s41232-023-00256-8 (2023).

17 Sun, Z. *et al.* Critical role of MXRA7 in differentiation blockade in human acute promyelocytic leukemia cells. *Experimental hematology*, doi:10.1016/j.exphem.2023.07.001 (2023).

18 Tossetta, G., Piani, F., Borghi, C. & Marzioni, D. Role of CD93 in Health and Disease. *Cells* **12**, doi:10.3390/cells12131778 (2023).
19 Yang, J. *et al.* Sequential genome-wide CRISPR-Cas9 screens identify genes regulating cell-surface expression of tetraspanins. *Cell reports* **42**, 112065, doi:10.1016/j.celrep.2023.112065 (2023).
20 Yi, X. *et al.* Ribosomal protein L22-like1 promotes prostate cancer progression by activating PI3K/Akt/mTOR signalling pathway. *Journal of cellular and molecular medicine* **27**, 403-411, doi:10.1111/jcmm.17663 (2023).
21 Contreras, O., Rossi, F. M. V. & Theret, M. Origins, potency, and heterogeneity of skeletal muscle fibro-adipogenic progenitors-time for new definitions. *Skeletal muscle* **11**, 16, doi:10.1186/s13395-021-00265-6 (2021).
22 Coulis, G. *et al.* Single-cell and spatial transcriptomics identify a macrophage population associated with skeletal muscle fibrosis. *Science advances* **9**, eadd9984, doi:10.1126/sciadv.add9984 (2023).
23 Ding, J., Li, Q., Liang, F., Bhattarai, S. & Liu, Q. Mechanical ventilation regulated the differentiation and proliferation of diaphragm satellite cells. *Frontiers in bioscience* **26**, 1013-1018, doi:10.52586/5005 (2021).
24 Edelman, B. L. & Redente, E. F. Isolation and Characterization of Mouse Fibroblasts. *Methods in molecular biology* **1809**, 59-67, doi:10.1007/978-1-4939-8570-8_5 (2018).
25 Wang, X. *et al.* Diverse effector and regulatory functions of fibro/adipogenic progenitors during skeletal muscle fibrosis in muscular dystrophy. *iScience* **26**, 105775, doi:10.1016/j.isci.2022.105775 (2023).
26 Wohlgemuth, R. P. *et al.* The extracellular matrix of dystrophic mouse diaphragm accounts for the majority of its passive stiffness and is resistant to collagenase digestion. *Matrix biology plus* **18**, 100131, doi:10.1016/j.mbplus.2023.100131 (2023).
27 Zhang, W., Liu, Y. & Zhang, H. Extracellular matrix: an important regulator of cell functions and skeletal muscle development. *Cell & bioscience* **11**, 65, doi:10.1186/s13578-021-00579-4 (2021).
28 Alabi, B. R., LaRanger, R. & Shay, J. W. Decellularized mice colons as models to study the contribution of the extracellular matrix to cell behavior and colon cancer progression. *Acta biomaterialia* **100**, 213-222, doi:10.1016/j.actbio.2019.09.033 (2019).
29 Al-Habeeb, F. *et al.* Human antigen R promotes lung fibroblast differentiation to myofibroblasts and increases extracellular matrix production. *Journal of cellular physiology* **236**, 6836-6851, doi:10.1002/jcp.30380 (2021).
30 Bai, D. *et al.* A conserved TGFbeta1/HuR feedback circuit regulates the fibrogenic response in fibroblasts. *Cellular signalling* **24**, 1426-1432, doi:10.1016/j.cellsig.2012.03.003 (2012).
31 Biehl, A. *et al.* Towards a standardized multi-tissue decellularization protocol for the derivation of extracellular matrix materials. *Biomaterials science* **11**, 641-654, doi:10.1039/d2bm01012g (2023).
32 Manini, A., Abati, E., Nuredini, A., Corti, S. & Comi, G. P. Adeno-Associated Virus (AAV)-Mediated Gene Therapy for Duchenne Muscular Dystrophy: The Issue of Transgene Persistence. *Frontiers in neurology* **12**, 814174, doi:10.3389/fneur.2021.814174 (2021).
33 Woodhoo, A. *et al.* Human antigen R contributes to hepatic stellate cell activation and liver fibrosis. *Hepatology* **56**, 1870-1882, doi:10.1002/hep.25828 (2012).
34 Stefanati, M., Torrente, Y. & Rodriguez Matas, J. F. Effect of myofibril architecture on the active contraction of dystrophic muscle. A mathematical model. *Journal of the mechanical behavior of biomedical materials* **114**, 104214, doi:10.1016/j.jmbbm.2020.104214 (2021).
35 Bernau, K. *et al.* Tensin 1 Is Essential for Myofibroblast Differentiation and Extracellular Matrix Formation. *American journal of respiratory cell and molecular biology* **56**, 465-476, doi:10.1165/rcmb.2016-0104OC (2017).
36 Ebbert, M. T. W. *et al.* Systematic analysis of dark and camouflaged genes reveals disease-relevant genes hiding in plain sight. *Genome biology* **20**, 97, doi:10.1186/s13059-019-1707-2 (2019).
37 Elangkovan, N. & Dickson, G. Gene Therapy for Duchenne Muscular Dystrophy. *Journal of neuromuscular diseases* **8**, S303-S316, doi:10.3233/JND-210678 (2021).

38 Gilchrist, S. C., Ontell, M. P., Kochanek, S. & Clemens, P. R. Immune response to full-length dystrophin delivered to Dmd muscle by a high-capacity adenoviral vector. *Molecular therapy : the journal of the American Society of Gene Therapy* **6**, 359-368, doi:10.1006/mthe.2002.0675 (2002).
39 Ho, P. P. *et al.* Engineered DNA plasmid reduces immunity to dystrophin while improving muscle force in a model of gene therapy of Duchenne dystrophy. *Proceedings of the National Academy of Sciences of the United States of America* **115**, E9182-E9191, doi:10.1073/pnas.1808648115 (2018).
40 Nasrallah, R. *et al.* A distal enhancer at risk locus 11q13.5 promotes suppression of colitis by T(reg) cells. *Nature* **583**, 447-452, doi:10.1038/s41586-020-2296-7 (2020).
41 Olsen, J. V. *et al.* Global, in vivo, and site-specific phosphorylation dynamics in signaling networks. *Cell* **127**, 635-648, doi:10.1016/j.cell.2006.09.026 (2006).
42 Santiago-Garcia, J., Mas-Oliva, J., Saavedra, D. & Zarain-Herzberg, A. Analysis of mRNA expression and cloning of a novel plasma membrane Ca(2+)-ATPase splice variant in human heart. *Molecular and cellular biochemistry* **155**, 173-182, doi:10.1007/BF00229314 (1996).
43 Srinivasan, J. *et al.* Age-Related Changes in Thymic Central Tolerance. *Frontiers in immunology* **12**, 676236, doi:10.3389/fimmu.2021.676236 (2021).
44 Watanabe, K., Yokota, K., Yoshida, K., Matsumoto, A. & Iwamoto, S. A novel upstream transcription factor 1 target gene N4bp2l1 that regulates adipogenesis. *Biochemistry and biophysics reports* **20**, 100676, doi:10.1016/j.bbrep.2019.100676 (2019).
45 Saenz, A. *et al.* Gene expression profiling in limb-girdle muscular dystrophy 2A. *PLoS One* **3**, e3750, doi:10.1371/journal.pone.0003750 (2008).
46 Ogura, Y., Tajrishi, M. M., Sato, S., Hindi, S. M. & Kumar, A. Therapeutic potential of matrix metalloproteinases in Duchenne muscular dystrophy. *Frontiers in cell and developmental biology* **2**, 11, doi:10.3389/fcell.2014.00011 (2014).
47 Soslow, J. H. *et al.* The Role of Matrix Metalloproteinases and Tissue Inhibitors of Metalloproteinases in Duchenne Muscular Dystrophy Cardiomyopathy. *Journal of cardiac failure* **25**, 259-267, doi:10.1016/j.cardfail.2019.02.006 (2019).
48 Mesnard-Rouiller, L., Bismuth, J., Wakkach, A., Poea-Guyon, S. & Berrih-Aknin, S. Thymic myoid cells express high levels of muscle genes. *Journal of neuroimmunology* **148**, 97-105, doi:10.1016/j.jneuroim.2003.11.013 (2004).
49 Alex, S. *et al.* Short-chain fatty acids stimulate angiopoietin-like 4 synthesis in human colon adenocarcinoma cells by activating peroxisome proliferator-activated receptor gamma. *Molecular and cellular biology* **33**, 1303-1316, doi:10.1128/MCB.00858-12 (2013).
50 Arimochi, H., Sasaki, Y., Kitamura, A. & Yasutomo, K. Differentiation of preadipocytes and mature adipocytes requires PSMB8. *Scientific reports* **6**, 26791, doi:10.1038/srep26791 (2016).
51 den Besten, G. *et al.* Short-Chain Fatty Acids Protect Against High-Fat Diet-Induced Obesity via a PPARgamma-Dependent Switch From Lipogenesis to Fat Oxidation. *Diabetes* **64**, 2398-2408, doi:10.2337/db14-1213 (2015).
52 Mukherjee, P., Chattopadhyay, A. & Fogelman, A. M. The role of the small intestine in modulating metabolism and inflammation in atherosclerosis and cancer. *Current opinion in lipidology* **30**, 383-387, doi:10.1097/MOL.0000000000000629 (2019).
53 Rath, E. & Haller, D. Intestinal epithelial cell metabolism at the interface of microbial dysbiosis and tissue injury. *Mucosal immunology* **15**, 595-604, doi:10.1038/s41385-022-00514-x (2022).
54 Boca, S. M. *et al.* Correction: Discovery of Metabolic Biomarkers for Duchenne Muscular Dystrophy within a Natural History Study. *PLoS One* **11**, e0159895, doi:10.1371/journal.pone.0159895 (2016).
55 Clarke, S. F. *et al.* Exercise and associated dietary extremes impact on gut microbial diversity. *Gut* **63**, 1913-1920, doi:10.1136/gutjnl-2013-306541 (2014).
56 Coenen-Stass, A. M. *et al.* Identification of novel, therapy-responsive protein biomarkers in a mouse model of Duchenne muscular dystrophy by aptamer-based serum proteomics. *Scientific reports* **5**, 17014, doi:10.1038/srep17014 (2015).

57 D'Amico, D. *et al.* Impact of the Natural Compound Urolithin A on Health, Disease, and Aging. *Trends in molecular medicine* **27**, 687-699, doi:10.1016/j.molmed.2021.04.009 (2021).
58 Goemans, N. *et al.* Comparison of ambulatory capacity and disease progression of Duchenne muscular dystrophy subjects enrolled in the drisapersen DMD114673 study with a matched natural history cohort of subjects on daily corticosteroids. *Neuromuscular disorders : NMD* **27**, 203-213, doi:10.1016/j.nmd.2016.11.013 (2017).
59 Griffin, J. L. *et al.* Metabolic profiling of genetic disorders: a multitissue (1)H nuclear magnetic resonance spectroscopic and pattern recognition study into dystrophic tissue. *Analytical biochemistry* **293**, 16-21, doi:10.1006/abio.2001.5096 (2001).
60 Han, X. *et al.* Identification of Auxiliary Biomarkers and Description of the Immune Microenvironmental Characteristics in Duchenne Muscular Dystrophy by Bioinformatical Analysis and Experiment. *Frontiers in neuroscience* **16**, 891670, doi:10.3389/fnins.2022.891670 (2022).
61 Hathout, Y. *et al.* Large-scale serum protein biomarker discovery in Duchenne muscular dystrophy. *Proceedings of the National Academy of Sciences of the United States of America* **112**, 7153-7158, doi:10.1073/pnas.1507719112 (2015).
62 Llano-Diez, M. *et al.* Digital PCR quantification of miR-30c and miR-181a as serum biomarkers for Duchenne muscular dystrophy. *Neuromuscular disorders : NMD* **27**, 15-23, doi:10.1016/j.nmd.2016.11.003 (2017).
63 Luan, P. *et al.* Urolithin A improves muscle function by inducing mitophagy in muscular dystrophy. *Science translational medicine* **13**, doi:10.1126/scitranslmed.abb0319 (2021).
64 Martins-Bach, A. B., Bloise, A. C., Vainzof, M. & Rahnamaye Rabbani, S. Metabolic profile of dystrophic mdx mouse muscles analyzed with in vitro magnetic resonance spectroscopy (MRS). *Magnetic resonance imaging* **30**, 1167-1176, doi:10.1016/j.mri.2012.04.003 (2012).
65 Marullo, A. L. & O'Halloran, K. D. Microbes, metabolites and muscle: Is the gut-muscle axis a plausible therapeutic target in Duchenne muscular dystrophy? *Experimental physiology* **108**, 1132-1143, doi:10.1113/EP091063 (2023).
66 Mizuno, H. *et al.* Identification of muscle-specific microRNAs in serum of muscular dystrophy animal models: promising novel blood-based markers for muscular dystrophy. *PLoS One* **6**, e18388, doi:10.1371/journal.pone.0018388 (2011).
67 Nguyen, D. T. *et al.* Pharos: Collating protein information to shed light on the druggable genome. *Nucleic acids research* **45**, D995-D1002, doi:10.1093/nar/gkw1072 (2017).
68 Rodriguez, M. C. & Tarnopolsky, M. A. Patients with dystrophinopathy show evidence of increased oxidative stress. *Free radical biology & medicine* **34**, 1217-1220, doi:10.1016/s0891-5849(03)00141-2 (2003).
69 Schepper, J. D. *et al.* Involvement of the Gut Microbiota and Barrier Function in Glucocorticoid-Induced Osteoporosis. *Journal of bone and mineral research : the official journal of the American Society for Bone and Mineral Research* **35**, 801-820, doi:10.1002/jbmr.3947 (2020).
70 Scholer, N., Langer, C., Dohner, H., Buske, C. & Kuchenbauer, F. Serum microRNAs as a novel class of biomarkers: a comprehensive review of the literature. *Experimental hematology* **38**, 1126-1130, doi:10.1016/j.exphem.2010.10.004 (2010).
71 Sheils, T. *et al.* How to Illuminate the Druggable Genome Using Pharos. *Current protocols in bioinformatics* **69**, e92, doi:10.1002/cpbi.92 (2020).
72 Szigyarto, C. A. & Spitali, P. Biomarkers of Duchenne muscular dystrophy: current findings. *Degenerative neurological and neuromuscular disease* **8**, 1-13, doi:10.2147/DNND.S121099 (2018).
73 Terrill, J. R., Radley-Crabb, H. G., Grounds, M. D. & Arthur, P. G. N-Acetylcysteine treatment of dystrophic mdx mice results in protein thiol modifications and inhibition of exercise induced myofibre necrosis. *Neuromuscular disorders : NMD* **22**, 427-434, doi:10.1016/j.nmd.2011.11.007 (2012).
74 Touboul, D., Brunelle, A., Halgand, F., De La Porte, S. & Laprevote, O. Lipid imaging by gold cluster time-of-flight secondary ion mass spectrometry: application to Duchenne muscular dystrophy. *Journal of lipid research* **46**, 1388-1395, doi:10.1194/jlr.M500058-JLR200 (2005).

75 Wang, M. *et al.* Gut microbiota mediated the therapeutic efficacies and the side effects of prednisone in the treatment of MRL/lpr mice. *Arthritis research & therapy* **23**, 240, doi:10.1186/s13075-021-02620-w (2021).
76 Heimli, M. *et al.* Multimodal human thymic profiling reveals trajectories and cellular milieu for T agonist selection. *Frontiers in immunology* **13**, 1092028, doi:10.3389/fimmu.2022.1092028 (2022).
77 Kehrmann, J. *et al.* Depletion of Foxp3(+) regulatory T cells is accompanied by an increase in the relative abundance of Firmicutes in the murine gut microbiome. *Immunology* **159**, 344-353, doi:10.1111/imm.13158 (2020).
78 Le, J., Ha, V. L., Luong, A. & Parekh, C. Processing Human Thymic Tissue for Single Cell RNA-Seq. *STAR protocols* **1**, 100090, doi:10.1016/j.xpro.2020.100090 (2020).
79 Liu, Y., Tran, D. Q., Lindsey, J. W. & Rhoads, J. M. The Association of Gut Microbiota and Treg Dysfunction in Autoimmune Diseases. *Advances in experimental medicine and biology* **1278**, 191-203, doi:10.1007/978-981-15-6407-9_10 (2021).
80 Pandiyan, P. *et al.* Microbiome Dependent Regulation of T(regs) and Th17 Cells in Mucosa. *Frontiers in immunology* **10**, 426, doi:10.3389/fimmu.2019.00426 (2019).
81 Park, J. E. *et al.* A cell atlas of human thymic development defines T cell repertoire formation. *Science* **367**, doi:10.1126/science.aay3224 (2020).
82 Wiechers, C. *et al.* The microbiota is dispensable for the early stages of peripheral regulatory T cell induction within mesenteric lymph nodes. *Cellular & molecular immunology* **18**, 1211-1221, doi:10.1038/s41423-021-00647-2 (2021).
83 Zheng, Y. *et al.* Role of conserved non-coding DNA elements in the Foxp3 gene in regulatory T-cell fate. *Nature* **463**, 808-812, doi:10.1038/nature08750 (2010).
84 Liang, Z., Dong, X., Zhang, Z., Zhang, Q. & Zhao, Y. Age-related thymic involution: Mechanisms and functional impact. *Aging cell* **21**, e13671, doi:10.1111/acel.13671 (2022).
85 Araki, T. *et al.* Normal thymus in adults: appearance on CT and associations with age, sex, BMI and smoking. *European radiology* **26**, 15-24, doi:10.1007/s00330-015-3796-y (2016).
86 Gioulbasani, M. & Tsagaratou, A. Defining iNKT Cell Subsets and Their Function by Flow Cytometry. *Current protocols* **3**, e838, doi:10.1002/cpz1.838 (2023).
87 Simanovsky, N., Hiller, N., Loubashevsky, N. & Rozovsky, K. Normal CT characteristics of the thymus in adults. *European journal of radiology* **81**, 3581-3586, doi:10.1016/j.ejrad.2011.12.015 (2012).
88 Anderson, J. *et al.* Interleukin 1 Receptor-Like 1 Protein (ST2) is a Potential Biomarker for Cardiomyopathy in Duchenne Muscular Dystrophy. *Pediatric cardiology* **38**, 1606-1612, doi:10.1007/s00246-017-1703-9 (2017).
89 Lemos, J. P. *et al.* T cell biology in neuromuscular disorders: a focus on Duchenne Muscular Dystrophy and Amyotrophic Lateral Sclerosis. *Frontiers in immunology* **14**, 1202834, doi:10.3389/fimmu.2023.1202834 (2023).
90 Chung Liang, L., Sulaiman, N. & Yazid, M. D. A Decade of Progress in Gene Targeted Therapeutic Strategies in Duchenne Muscular Dystrophy: A Systematic Review. *Frontiers in bioengineering and biotechnology* **10**, 833833, doi:10.3389/fbioe.2022.833833 (2022).
91 Jayaraman, A. & Pettersson, S. When dysbiosis meets dystrophy: an unwanted gut-muscle connection. *EMBO molecular medicine* **15**, e17324, doi:10.15252/emmm.202217324 (2023).
92 Nowak, G. & Bakajsova, D. Protein kinase C-alpha activation promotes recovery of mitochondrial function and cell survival following oxidant injury in renal cells. *American journal of physiology. Renal physiology* **303**, F515-526, doi:10.1152/ajprenal.00072.2012 (2012).
93 Consalvi, S. *et al.* Preclinical studies in the mdx mouse model of duchenne muscular dystrophy with the histone deacetylase inhibitor givinostat. *Molecular medicine* **19**, 79-87, doi:10.2119/molmed.2013.00011 (2013).
94 Przewlocka, K., Folwarski, M., Kazmierczak-Siedlecka, K., Skonieczna-Zydecka, K. & Kaczor, J. J. Gut-Muscle AxisExists and May Affect Skeletal Muscle Adaptation to Training. *Nutrients* **12**, doi:10.3390/nu12051451 (2020).

95 Rahimov, F. & Kunkel, L. M. The cell biology of disease: cellular and molecular mechanisms underlying muscular dystrophy. *The Journal of cell biology* **201**, 499-510, doi:10.1083/jcb.201212142 (2013).
96 Barnicle, A., Seoighe, C., Greally, J. M., Golden, A. & Egan, L. J. Inflammation-associated DNA methylation patterns in epithelium of ulcerative colitis. *Epigenetics* **12**, 591-606, doi:10.1080/15592294.2017.1334023 (2017).
97 Das, A. S. *et al.* Post-transcriptional regulation of C-C motif chemokine ligand 2 expression by ribosomal protein L22 during LPS-mediated inflammation. *The FEBS journal* **287**, 3794-3813, doi:10.1111/febs.15362 (2020).
98 Fathi, E., Yarbro, J. M. & Homayouni, R. NIPSNAP protein family emerges as a sensor of mitochondrial health. *Bioessays* **43**, e2100014, doi:10.1002/bies.202100014 (2021).
99 Wu, S., Qiu, S., Chen, W., Ding, L. & Wu, L. Prognostic Signature GXYLT2 Is Correlated with Immune Infiltration in Bladder Cancer. *Disease markers* **2022**, 5081413, doi:10.1155/2022/5081413 (2022).
100 El-Shafey, A. F., Armstrong, A. E., Terrill, J. R., Grounds, M. D. & Arthur, P. G. Screening for increased protein thiol oxidation in oxidatively stressed muscle tissue. *Free radical research* **45**, 991-999, doi:10.3109/10715762.2011.590136 (2011).
101 Hung, C. F., Wilson, C. L., Chow, Y. H. & Schnapp, L. M. Role of integrin alpha8 in murine model of lung fibrosis. *PLoS One* **13**, e0197937, doi:10.1371/journal.pone.0197937 (2018).
102 Terrill, J. R. *et al.* Levels of inflammation and oxidative stress, and a role for taurine in dystropathology of the Golden Retriever Muscular Dystrophy dog model for Duchenne Muscular Dystrophy. *Redox biology* **9**, 276-286, doi:10.1016/j.redox.2016.08.016 (2016).
103 Wu, C. *et al.* Gut Microbiota Influence Lipid Metabolism of Skeletal Muscle in Pigs. *Frontiers in nutrition* **8**, 675445, doi:10.3389/fnut.2021.675445 (2021).
104 Villalta, S. A., Rosenberg, A. S. & Bluestone, J. A. The immune system in Duchenne muscular dystrophy: Friend or foe. *Rare diseases* **3**, e1010966, doi:10.1080/21675511.2015.1010966 (2015).
105 Domingues-Faria, C., Vasson, M. P., Goncalves-Mendes, N., Boirie, Y. & Walrand, S. Skeletal muscle regeneration and impact of aging and nutrition. *Ageing research reviews* **26**, 22-36, doi:10.1016/j.arr.2015.12.004 (2016).
106 Eby, S. F. *et al.* Shear wave elastography of passive skeletal muscle stiffness: influences of sex and age throughout adulthood. *Clinical biomechanics* **30**, 22-27, doi:10.1016/j.clinbiomech.2014.11.011 (2015).
107 Zhao, J., Huang, Y. & Yu, X. A Narrative Review of Gut-Muscle Axis and Sarcopenia: The Potential Role of Gut Microbiota. *International journal of general medicine* **14**, 1263-1273, doi:10.2147/IJGM.S301141 (2021).
108 Farini, A. *et al.* Microbiota dysbiosis influences immune system and muscle pathophysiology of dystrophin-deficient mice. *EMBO molecular medicine* **15**, e16244, doi:10.15252/emmm.202216244 (2023).
109 Quinlan, J. G. *et al.* Evolution of the mdx mouse cardiomyopathy: physiological and morphological findings. *Neuromuscular disorders : NMD* **14**, 491-496, doi:10.1016/j.nmd.2004.04.007 (2004).